Spinodal Decomposition of Polymer Mixtures: A Monte Carlo Simulation

A. Sariban† and K. Binder*

Institut für Physik, Johannes Gutenberg Universität Mainz, D-6500 Mainz, Postfach 3980, Federal Republic of Germany

Received April 13, 1990

ABSTRACT: The initial stages of phase separation are studied for a symmetrical lattice model of a polymer mixture, where both polymers A and B are modeled by self-avoiding walks of $N_A = N_B = N$ steps on the simple cubic lattice and a lattice site is taken by either an A monomer, a B monomer, or a solvent molecule (or a vacancy V, respectively), choosing a volume fraction $\phi_V = 0.6$. We study two cases of energy parameters, (i) $\epsilon = -\epsilon_{AA} = -\epsilon_{BB}$ (if two neighboring sites are taken by monomers of the same kind) and $\epsilon_{AB} = 0$ (if two neighboring sites are taken by monomers of different kind) and (ii) $\epsilon = \epsilon_{AB}$ and $\epsilon_{AA} = \epsilon_{BB} = 0$. For chain lengths $N = 8$ and 32 and volume fractions $\phi_A/(1 - \phi_V) = 0.5$ and 0.2, the system is quenched from the randomly mixed initial state ($\epsilon/k_BT = 0$) to various unstable states inside the spinodal, and the time evolution of various structure factors after the quench is monitored, as well as the time evolution of the chain radii and various types of nearest-neighbor contacts. It is shown that in case (i) also some segregation of solvent (vacancies) occurs, accompanied by a contraction of the chains, while in case (ii) the vacancies remain randonly distributed in the system, and the radii of the chains do not change significantly. In neither case can the data be accounted for by the linearized (Cahn-type) theory of spinodal decomposition. We suggest that this theory should hold only for much longer chains and rather shallow quenches. Performing runs also in the grand-canonical ensemble of the mixture, long-lived metastable states are identified but only in the close neighborhood of the binodal curve. Consequences of our results for the interpretation of experiments are briefly discussed.

1. Introduction

By spinodal decomposition of a polymer mixture, one means the phase-separation process induced by the "quench" (Figure 1) from a state where the system is miscible to an unstable state inside the miscibility gap (see refs 1–5 for recent reviews). For a system exhibiting an upper critical solution temperature (UCST), by quench we mean a sudden cooling of the system from the one-phase region into the two-phase region, while for a system with a lower critical solution temperature (LCST) the quench is a sudden heating. In both cases, the initial rather homogeneous state will decay by the growth of concentration fluctuations. The initial length scale, $\lambda_m(t=0)$, of these concentration inhomogeneities typically is of the same order of magnitude as the size of the coils, while at later times t after the quench the inhomogeneous concentration distribution coarsens, $\lambda_m(t\to\infty) \to \infty$. This process is of fundamental interest for the theoretical understanding of phase transitions and their kinetics,[3-5] and polymer mixtures are rather ideally suited model systems for the experimental study of these phenomena: for melts of long flexible linear macromolecules, all diffusion processes are so slow that also very early stages of the decomposition process can actually be observed,[6-15] and light scattering,[6-11] neutron scattering,[12-14] and scattering of X-rays[15] are available as tools that yield detailed information on the collective structure factor, which is essentially the Fourier transform of the correlation function of these concentration fluctuations.

In addition, it has been suggested that spinodal decomposition of polymer blends may have important technological applications, using processing techniques by which one can *control the morphology* of the resulting two-phase structures: this may be achieved by freezing the structure at a given time after the start of the phase separation by suddenly cooling it far below the glass transition temperature[16] or by activating a cross-linking agent,[17] etc.

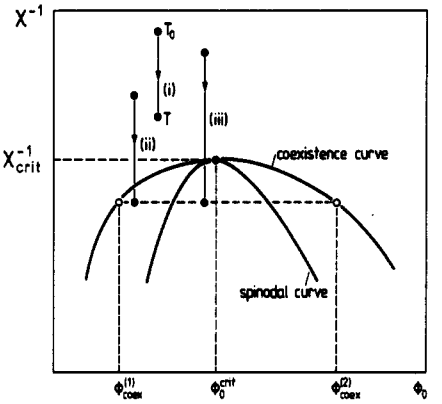

Figure 1. Schematic phase diagram of a polymer mixture, choosing the volume fraction ϕ_0 of one component and the inverse Flory–Huggins parameter, χ^{-1}, as the basic variables. A critical point of unmixing occurs at a volume fraction ϕ_0^{crit} and at a value χ_{crit} of the (temperature-dependent) effective interaction parameter χ. Note that in this representation the phase diagram applies to both LCST and UCST systems (cf. text). Full curves show the coexistence curve, which separates the one-phase region (above) from the two-phase region (below), and the spinodal curve, which is thought to separate the unstable region (below) from the metastable region (in between spinodal and coexistence curves). Also, three types of quenching experiments (i)–(iii) from an initial state at temperature T_0 to other states at a temperature T are indicated.

Clearly, a detailed theoretical understanding of these processes enabling us to predict the detailed kinetic behavior of such unmixing processes would be very desirable. The theory of spinodal decomposition for polymer mixtures has been considered by various authors[3,18-25] but is only incompletely understood. This is no surprise at all: even for small molecule mixtures, nonlinear effects prevent a satisfactory theoretical description of spinodal decomposition;[5,26] in addition, the dynamics of homopolymeric melts poses already very difficult problems.[27] While there is no reason to assume that late-stage spinodal decomposition for polymers is simpler than it is for small-

† Present address: Institut für Physikalische Chemie, Technische Hochschule Darmstadt, D-6100 Darmstadt, FRG.

0024-9297/91/2224-0578$02.50/0

molecule mixtures, one very attractive feature of polymer mixtures is the prediction[3,20,21] that polymers should have a well-defined regime of early times after the quench where the linearized theory of spinodal decomposition[3,28,29] holds. In fact, there is some experimental evidence for this prediction.[7-11] For small-molecule mixtures, it is argued that nonlinear effects are very important already in the initial configuration,[21] and furthermore due to the quicker interdiffusion of small molecules, the very early stages of phase separation are not experimentally observable. However, even on the level of linearized treatments[18-21] of spinodal decomposition, there are problems: it is controversial how the generalized Onsager coefficient, $\Lambda(\vec{q})$, describing interdiffusion of ideal randomly mixed polymers at wavelength $\lambda = 2\pi/q$ behaves; also the relation of $\Lambda(\vec{q}\rightarrow 0)$ to self-diffusion coefficients of the two types of chains forming the mixture is controversial.[3,30-38]

In view of all these problems, Monte Carlo simulations of spinodal decomposition should be very helpful: for spinodal decomposition of metallic alloys, Monte Carlo simulations have played a central role in clarifying the accuracy of various theories and checking out various theoretical predictions.[5,39-43] Of course, due to the internal degrees of freedom of long polymer chains already the simulation of homopolymer melts is very difficult.[44,46] Previous simulations of spinodal decomposition of polymers in $d = 2$ dimensions[47] and in $d = 3$ dimensions[48] only have the character of feasibility studies (considering a single quench depth and a single chain length, $N = 10^4$[47] or $N = 32$,[48] respectively), rather than a systematic investigation of the problem.

In the present paper, we hence extend our preliminary previous work[48] studying now the effect of varying both quench depth and chain length, and we also present the first Monte Carlo results for quenches at off-critical concentration. Since for our simple cubic lattice model static properties such as binodal[49] and spinodal curves[50] have been obtained in previous work, a quantitative analysis of the Monte Carlo "data" is possible without unknown fitting parameters.

The outline of our paper is as follows. Section 2 contains a brief summary of the results of the linear theory of spinodal decomposition,[3,20] which will be used for later comparison. Section 3 briefly describes the simulated model and summarizes the pertinent static properties obtained in previous simulations.[49,50] Section 4 describes our simulation results for a model with repulsive interactions between unlike monomers ($\epsilon = \epsilon_{AB} > 0$), while Section 5 describes corresponding results for a model with attractive interactions between monomers of the same kind ($\epsilon = -\epsilon_{AA} = -\epsilon_{BB} > 0$). Since the simulated model[48-50] includes a (rather large) volume fraction, ϕ_V, of vacant sites (or solvent molecules, respectively), these two models behave in a very different manner, while for $\phi_V \rightarrow 0$ only the combination $\epsilon_{AB} - (\epsilon_{AA} + \epsilon_{BB})/2$ would matter and then both cases were identical. Section 6 then summarizes our conclusions and discusses a possible relation to experimental work. Finally, an appendix describes our attempts to simulate metastable homogeneous states in between the spinodal and binodal curves, applying the same grand-canonical ensemble techniques as have been appropriate for the study of equilibrium properties.

2. Linearized Theory of Spinodal Decomposition for Polymer Mixtures

In this section, we disregard the fact that the simulated model really is a ternary system containing vacancies in addition to the two kinds of polymers: we only consider an incompressible binary polymer mixture, assuming that the actual ternary system can be mapped onto the binary one by a suitable rescaling of parameters, as will be discussed below. Since the theory has been discussed elsewhere in detail,[20] we here summarize only the main results.

The starting point of the description is a Flory–Huggins lattice model[51] of the polymer mixture, where a local concentration variable $\phi_A{}^i = 1$ if lattice site i is taken by an A monomer and otherwise zero and $\phi_B{}^i = 1$ if it is taken by a B monomer and otherwise zero. Then the time-dependent collective structure function of an $L \times L \times L$ lattice (we measure all lengths henceforth in units of the lattice spacing) is given by

$$S(\vec{q},t) \equiv \langle \{ \sum_j \exp(i\vec{q}\cdot\vec{R}_j)[\phi_B{}^j(t) - \phi_A{}^j(t) - \langle \phi_B{}^j - \phi_A{}^j \rangle]\}^2 \rangle / L^3 \quad (1)$$

Here $\langle \cdots \rangle$ denotes a thermal statistical average, and we display a time argument for this equal-time structure factor, since we consider a quench at time $t = 0$ (Figure 1), and thus the system for $t > 0$ is out of thermal equilibrium. Of course, the average relative composition of the considered mixture $\phi_0 = \langle \phi_A{}^j \rangle / \langle \phi_B{}^j + \phi_A{}^j \rangle$ is conserved in the phase-separation process following this quench.

Now the linearized theory of spinodal decomposition implies an exponential variation of $S(\vec{q},t)$ with time

$$S(\vec{q},t) - S(\vec{q},t=0) = [S_T{}^{\mathrm{coll}}(\vec{q}) - S(\vec{q},t=0)][1 - \exp\{2R(\vec{q})t\}] \quad (2)$$

where the initial structure factor $S(\vec{q},t=0) = S_{T_0}{}^{\mathrm{coll}}(\vec{q})$, i.e., the collective structure function describing the scattering under wavevector $\vec{q}$ from concentration fluctuations in thermal equilibrium at the initial temperature T_0. According to the random-phase approximation, $S_T{}^{\mathrm{coll}}(\vec{q})$ is given by[52]

$$\frac{1}{S_T{}^{\mathrm{coll}}(\vec{q})} = \frac{1}{\phi_0 S_A(\vec{q})} + \frac{1}{(1-\phi_0) S_B(\vec{q})} - 2\chi(T) \quad (3)$$

where $\chi(T)$ is the Flory–Huggins parameter (we display here explicitly only an unspecified temperature dependence, but it may also depend on ϕ_0[53]) and $S_A(\vec{q})$ and $S_B(\vec{q})$ are the single-chain structure factors of the two types of chains. Note that eq 3 assumes that $S_A(\vec{q})$ and $S_B(\vec{q})$ are strictly independent of both T and ϕ_0, which in general is not true, at least not for the model treated in our simulation.[49,54] We shall return to this problem in section 5 but remark that also eq 3 is at best qualitatively accurate for the model introduced in section 3.[50] If the chain configurations are ideal, the single-chain structure factors $S_A(\vec{q})$ and $S_B(\vec{q})$ can be expressed in terms of the well-known Debye function $f_D(x)$[51,52]

$$S_A(\vec{q}) = N_A f_D\left(\frac{1}{6} N_A \sigma_A{}^2 q^2\right), \quad S_B(\vec{q}) = N_B f_D\left(\frac{1}{6} N_B \sigma_B{}^2 q^2\right) \quad (4)$$

where

$$f_D(x) = (2/x)\{1 - [1 - \exp(-x)]/x\} \underset{x\rightarrow 0}{\approx} 1 - x/3 \quad (5)$$

where the chain lengths of the two polymers A and B are denoted by N_A and N_B, and the size of their effective units, σ_A and σ_B.

The rate $R(\vec{q})$ describing in eq 2 the variation of $S(\vec{q},t)$ with time is given by[20]

$$R(\vec{q}) = -q^2 \Lambda(\vec{q}) / S_T{}^{\mathrm{coll}}(\vec{q}) \quad (6)$$

where $\Lambda(\vec{q})$ is a generalized Onsager coefficient that will be discussed later.

If we would consider a quench with a final state above the spinodal curve in Figure 1 [case (i) or case (ii), respectively], we would have $S_T^{coll}(\vec{q}) > 0$ and hence $R(\vec{q}) < 0$ for all q. Then eq 2 simply describes an exponential decay of the correlations contained in the initial state, and the system smoothly relaxes toward its new equilibrium, described by the structure factor $S_T^{coll}(\vec{q})$. Spinodal decomposition occurs for the quench (iii) in Figure 1 which crosses the spinodal curve $\chi = \chi_{sp}(T)$, which follows from eq 3 from the condition $1/S_T^{coll}(\vec{q}\to 0) = 0$; i.e.

$$\chi_{sp}(T) = \frac{1}{2}\left[\frac{1}{\phi_0 N_A} + \frac{1}{(1-\phi_0)N_B}\right] \tag{7}$$

In the unstable regime, where $\chi > \chi_{sp}(T)$, we have $S_T^{coll}(\vec{q}) < 0$ for $0 < q < q_c$, where now q_c is given by the condition $1/S_T^{coll}(\vec{q}) = 0$. For a symmetric mixture for which $N_A = N_B = N_s$ and $\sigma_A = \sigma_B = \sigma$, which holds for the model treated in the following section, we then have, using $\chi_{crit} = 2/N_s$ and noting from eq 7 that $\chi_{sp}(T) = \chi_{crit}/[4\phi_0(1-\phi_0)]$ from eqs 3–5

$$f_D\left(\frac{1}{6}N_s\sigma^2 q_c^2\right) = [4\phi_0(1-\phi_0)\chi/\chi_{crit}]^{-1} = \chi_{sp}(T)/\chi \tag{8}$$

For a shallow quench, for which χ exceeds $\chi_{sp}(T)$ only slightly, the expansion of the Debye function in eq 5 may be used, and, hence, remembering $(1/6)N_s\sigma^2 = \langle R_{gyr}^2\rangle$, the gyration radius square of the coil

$$\frac{1}{3}\langle R_{gyr}^2\rangle q_c^2 = 1 - \chi_{sp}(T)/\chi \tag{9}$$

For a deep quench, on the other hand, for which $\chi \gg \chi_{sp}(T)$, we rather have to use the large x-approximation to $f_D(x)$, namely, $f_D(x) \approx 2/x$. This yields instead of eq 9

$$\langle R_{gyr}^2\rangle q_c^2/2 \approx \chi/\chi_{sp}(T) \tag{10}$$

For shallow quenches where $1 - \chi_{sp}(T)/\chi \ll 1$, eq 9 implies that $\langle R_{gyr}^2\rangle q_c^2 \ll 1$ and then in eq 6 the q-dependence of $\Lambda(\vec{q})$ may be neglected. Equations 3 and 6 then yield

$$R(\vec{q}) \approx 2\Lambda_0 q^2 \chi_{sp}(T)\frac{q_c^2\langle R_{gyr}^2\rangle}{3}(1 - q^2/q_c^2) \tag{11}$$

The position q_m where $R(\vec{q})$ is maximal then is $q_m = q_c/\sqrt{2}$ as in Cahn's treatment,[28] and the maximum growth rate should behave as

$$R(q_m) \approx \Lambda_0 q_m^4 \chi_{sp}(T)\langle R_{gyr}^2\rangle/6 \approx \Lambda_0 q_m^4\sigma^2/[36\chi_0(1-\chi_0)] \tag{12}$$

For deep quenches, on the other hand, the q-dependence of $\Lambda(q)$ crucially enters and this is the point where various theories differ.[18-20] We here quote the result of ref 20 only

$$q_m^2\langle R_{gyr}^2\rangle \approx (2\chi/\chi_{sp}(T))^{1/2}, \quad \chi \gg \chi_{sp}(T) \tag{13}$$

$$R(q_m) \approx 12(W/N_s^2)\chi/\chi_{sp}(T) \approx 6\frac{W}{N_s^2}q_m^4\langle R_{gyr}^2\rangle^2 \approx \frac{1}{6}W(\sigma q_m)^4 \tag{14}$$

where W is an effective monomer reorientation rate per unit time. Since[3] $\Lambda_0 \approx W\phi_0(1-\phi_0)\sigma^2$, eq 12 differs from eq 14 by a numerical factor only. These results will be compared to the computer simulation results in sections 4 and 5. Note that in our choice for Λ_0 we have assumed simply the Rouse model,[27] as is appropriate since our chains are rather short.

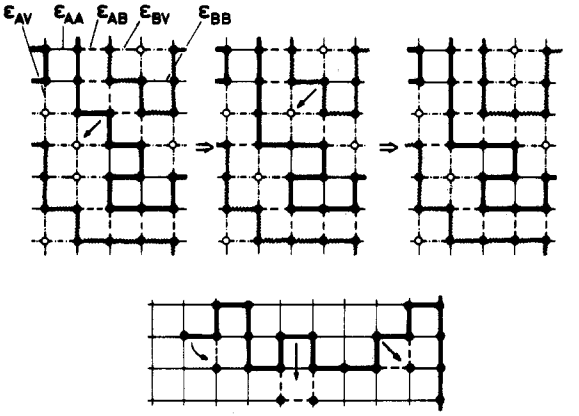

Figure 2. Schematic illustration of the dynamic Flory–Huggins lattice model of a polymer mixture. Lattice sites taken by monomers are indicated by full dots; lattice sites taken by vacancies are denoted by empty circles. Chains of type A are indicated by thick bonds between the monomers and B chains by wavy bonds. Nearest-neighbor bonds between monomers of the same kind (ϵ_{AA} and ϵ_{BB}) are denoted by full straight lines and those between monomers of a different kind (ϵ_{AB}) by broken lines. Interactions between monomers and vacancies (ϵ_{AV} and ϵ_{BV}) (which might as well represent solvent molecules rather than vacancies) are assumed to be zero in this work; they are denoted by dash-dotted lines in the figure. Dynamics is introduced into this model by random motion of single bonds (at the end of the chains), by a 90° "crankshaft" motion of three neighboring bonds (remember that we deal with the simple cubic lattice throughout rather than the square lattice, which here is used for illustrative purposes only), and by exchange of two neighboring bonds, which form an angle of 90° ("kink-jump" motion). These motions are indicated in the lower part of the figure. They must conform to the excluded-volume principle that each site can be taken by a single monomer only, and the bond energies ϵ_{AA}, ϵ_{BB}, and ϵ_{AB} must be taken into account via suitable transition probabilities, as is standard practice in Monte Carlo simulations of lattice models for polymers.[44] The upper part of the figure illustrates that by suitable succession of these random motions a lattice site previously taken by an A monomer later may be occupied by a B monomer.

3. Simulated Model and Its Static Properties

In the present paper, we are concerned with the same dynamic Flory–Huggins model of polymer mixtures as was used in previous work,[45,48-50,54,55] illustrated in Figure 2. We consider two choices of energy parameters, namely

$$\text{(i) } \epsilon_{AB} = \epsilon, \quad \epsilon_{AA} = \epsilon_{BB} = 0$$

$$\text{(ii) } \epsilon_{AB} = 0, \quad \epsilon_{AA} = \epsilon_{BB} = -\epsilon \tag{15}$$

In the absence of vacancies, the Flory–Huggins parameter χ used in section 2 according to the simplest version of the Flory–Huggins mean-field approximation[51] would be

$$\chi = \frac{z[\epsilon_{AB} - (\epsilon_{AA} + \epsilon_{BB})/2]}{k_B T} \tag{16}$$

where z is the coordination number of the lattice ($z = 6$ here), k_B is Boltzmann's constant, and T is the absolute temperature. Equation 15 suggests that the two cases (i) and (ii) are strictly equivalent, and this is rigorously true for $\phi_V = 0$ but not for $\phi_V \neq 0$. A simple generalization of Flory–Huggins theory for $\phi_V \neq 0$ yields[49,55]

$$\chi = \frac{z[\epsilon_{AB} - (\epsilon_{AA} + \epsilon_{BB})/2]}{k_B T}(1 - \phi_V) \tag{17}$$

which would imply that two cases (i) and (ii) both reduce

to the same result

$$\chi = z\epsilon(1 - \phi_V)/k_BT \tag{18}$$

Now the numerical results presented in ref 49 show that eqs 15–17 are rather inaccurate: (1) The above formulas assume that each chain with N bonds makes $(1 - \phi_V)zN$ contacts with monomers of other chains, which is a crude overestimate: due to excluded-volume effects on a local scale and the fact that intrachain contacts lead to a chain contraction[54] rather than to phase separation, the effective number of contacts $z_{eff}N$ is much smaller than zN, and hence z_{eff} rather than z should be used in eqs 15–17. (2) The vacancy concentration dependence of the effective χ parameter is much stronger than suggested by the factor $1 - \phi_V$ in eqs 16 and 17. (3) When an effective χ-parameter is fit to the simulation data, the parameter $k_BT\chi$ has both a weak temperature dependence and a slight dependence on the volume fraction $\phi_A = \langle\phi_A^i\rangle$.[49] (4) The two cases (i) and (ii) mentioned above are practically equivalent for very small ϕ_V, but this is no longer true for $\phi_V = 0.6$, the case considered here. This is seen from the fact that the critical temperatures found in both cases differ from each other; namely, e.g., for $N = 16$, one finds[49]

$$\epsilon/k_BT_c = 0.188 \text{ (i)}, \quad \epsilon/k_BT_c = 0.166 \text{ (ii)} \tag{19}$$

Thus for the present model, the dependence on the type of interaction {case (i) and case (ii) are two extreme possibilities for a whole class of choices for ϵ_{AB}, ϵ_{AA}, and ϵ_{BB}} is still a rather small effect, as far as the one-phase region and the critical region of the model is concerned. We shall see, however, that for spinodal decomposition where in a deep quench $\epsilon/k_BT \gg \epsilon/k_BT_c$ holds, nevertheless, pronounced differences between the two cases (i) and (ii) result.

Now a comparison between the phenomenological theory, as was outlined in section 2, and the simulated model is hampered by the fact that eqs 16 and 17 should not be used for a conversion of parameters. Similarly, one must neither identify the lattice spacing in Figure 2 with the segment length, σ, nor the number of segments, N_s, with the chain length N in the simulation, since the relation $\langle R_{gyr}^2\rangle = \sigma^2N_s/6$ would not be fulfilled. Rather one observes still a considerable swelling of the chains; i.e., the system corresponds to a semidilute solution with a blob size containing about 20 monomers. This is seen by the fact that the gyration radii are for $\phi_V = 0.6$[49]

$$\langle R_{gyr}^2\rangle_{N=8} \approx 1.75, \quad \langle R_{gyr}^2\rangle_{N=16} \approx 3.84, \quad \langle R_{gyr}^2\rangle_{N=32} \approx 9.1 \tag{20}$$

which all are in a crossover regime from the region where $\langle R_{gyr}^2\rangle \sim N^{2\nu}$ holds with $\nu \approx 0.59$ for small N to $\langle R_{gyr}^2\rangle \sim N$ for large N. In order to allow a meaningful comparison between the simulations and the phenomenological theory, we hence shall use the actual values of $\langle R_{gyr}^2\rangle$ in the normalization of the wavevector scale and use T/T_c as a parameter corresponding to χ_{crit}/χ in the normalization of the temperature scale.

Figure 3 shows the phase diagram of the model for case (ii) and the largest chain length studied ($N = 32$). Note that the spinodal curve was found from a *linear* extrapolation of the inverse collective structure factor $[S_T^{coll}(q=0)]^{-1}$ as obtained from the simulation versus ϵ/k_BT (for details see ref 50). Since the actual behavior of $[S_T^{coll}(q=0)]^{-1}$ as a function of ϵ/k_BT near ϵ/k_BT_c is nonlinear, reflecting a critical exponent γ different from unity,[49,50,55] one obtains the spurious result that a spinodal curve obtained from a strictly linear extrapolation for ϕ_A near ϕ_A^{crit} would lie slightly above the true T_c. This

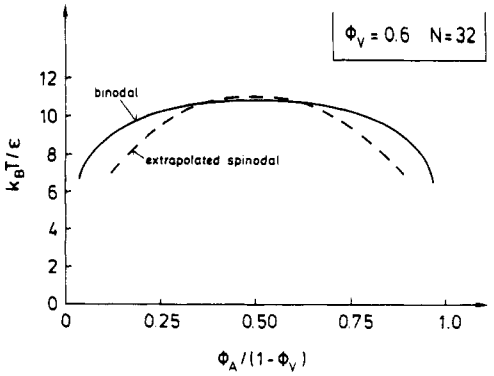

Figure 3. Phase diagram of the model polymer mixture displaying both the true coexistence curve (binodal) and the extrapolated spinodal, or the case $\phi_V = 0.6$, $N = 32$, $\epsilon_{AB} = 0$, and $\epsilon_{AA} = \epsilon_{BB} = -\epsilon$.

effect has also been seen in recent experiments on polystyrene–poly(vinyl methyl ether) mixtures.[56,57] This temperature region where the linear extrapolation fails gets smaller the larger the chain length N becomes, as a Ginzburg-type criterion shows.[20,52] Only for $N \to \infty$ the spinodal curve becomes well-defined,[20] while for the small N used in Figure 3, the dashed curve is only a rough estimate of the region in the phase diagram where a gradual transition from nucleation to spinodal decomposition should be expected.[3,5]

In our Monte Carlo simulations, we work with $L \times L \times L$ lattices, choosing $L = 40$ and periodic boundary conditions. This means that the structure function $S(\vec{q},t)$ defined in eq 1 is only well-defined for a set of discrete values $\vec{q}_\nu$ defined by

$$\vec{q}_\nu = \frac{2\pi}{L}(\nu_x,\nu_y,\nu_z), \quad \{\nu_x,\nu_y,\nu_z\} = 1, 2, 3, \ldots \tag{21}$$

The same fact is true for another structure function, which is sensitive against a possible polymer-vacancy phase separation; namely

$$S_\rho(\vec{q},t) \equiv \langle\{\sum_j \exp(i\vec{q}\cdot\vec{R}_j)[\phi_B^j(t) + \phi_A^j - \langle\phi_B^j + \phi_A^j\rangle]\}^2\rangle/L^3 \tag{22}$$

This quantity is the fourier transform of the correlation function of fluctuations in the density of polymers in the system; unlike eq 1 it does not distinguish between the two types of polymers A and B.

The initial configurations of the chains are prepared and relaxed in the same way as described in refs 49 and 55. In this relaxation part of the simulation, all energy parameters are put equal to zero, corresponding to an equilibration at infinite temperature, $T_0 \to \infty$. This implies that the initial structure factor $S_{T_0}(\vec{q})$ (eq 3) simply corresponds to the structure factor of single chains, since $\chi(T_0 \to \infty) = 0$. At $t = 0$ then the chosen value of ϵ/k_BT is switched on. This energy is felt in carrying out the trial moves shown in Figure 2 via the transition probability, $W = \exp(-\delta H/k_BT)$, if the energy change δH involved in a move is positive: the trial moves are carried out only if W exceeds a random number uniformly distributed between zero and one.[44–46] More details on this standard Monte Carlo procedure can be found in the reviews.[44–46]

One difficulty with this type of nonequilibrium Monte Carlo simulation is the fact that structure functions $S(\vec{q},t)$ and $S_\rho(\vec{q},t)$ for particular values of $\vec{q}$ are not self-averaging: this means the fluctuation of individual observations of the scattering (i.e., individual recordings of the quantity in braces in eqs 1 and 22, respectively) does not decrease with increasing size (L^3) of the simulated box but rather

is of order unity. In fact, the statistical average $\langle \cdots \rangle$ means in principle that one should perform an average over a large sample of equivalent runs, starting from different realizations of the initial equilibrated configuration and using different random numbers simulating the course of the "time" evolution. For the sake of computational economy, only of the order of 20–40, such runs have been carried out. To improve statistics of the structure function, we then perform the standard spherical average in $\vec{q}$ space; i.e., we define a $S(q,t)$ by summing $S(\vec{q},t)$ over all $\vec{q}$ vectors that lie in a shall between spheres with radii $(\nu - 1/2)\cdot(2\pi/L)$ and $(\nu + 1/2)(2\pi/L)$ and plot this value at $q_\nu = (2\pi/L)\nu$, for $\nu = 1, 2, 3, \ldots$.[39-43]

A comment should also be made on the conversion of time scales: the Monte Carlo "time" is measured in the units of attempted moves per "monomer" on the lattice. Very roughly, this means in the phenomenological theory that we measure time in units of the subunit reorientation rate, W. Of course, nothing hence can be said about the dependence of this quantity on temperature, local volume fraction, etc. In principle, it would also be possible to choose jump rates Γ_A and Γ_B for the motions shown in Figure 2 different for the two kinds of polymers. Such a parameter Γ_A/Γ_B has been introduced in recent simulations of interdiffusion in lattice gases[37] and polymer mixtures[38] and in a simulation of spinodal decomposition for an alloy model.[58] These rates enter as a prefactor in the transition probability, W, and since the latter must not exceed unity, it is the larger one of the two rate factors that controls the unit of time. Therefore, any ratio Γ_A/Γ_B appreciably different from unity distinctly slows down the simulation,[58] in units of the actually consumed CPU time. Therefore, in the present work we restrict attention to polymers with the same intrinsic mobilities, choosing $\Gamma_A = \Gamma_B = 1$ for all three types of motions shown in Figure 2: these attempted motions hence are always carried out if they do not violate the excluded-volume constraint and if $W = \mathrm{Min}\{\exp(-\delta H/k_BT),1\}$ exceeds the random number. Clearly, the "dynamics" of this Monte Carlo model is somewhat artificial when we compare it to the dynamics of real polymer melts: however, the simplification is in the same spirit, as the Flory–Huggins lattice model for the static properties of polymer mixtures drastically simplifies the problem. In fact, our approach is a rather natural extension of this model[49-53] to dynamics, and the motions included on the microscopic level (Figure 2) ensure that on time scales that are much larger than unity (the inverse jump rate in the absence of interactions is unity in our case) the Rouse model[27] is a good approximation to the dynamics of single chains in our model.[44-46] This fact is expected, of course, since the Monte Carlo process can be interpreted in terms of a master equation,[44,46] which is the discrete analogue of a description in terms of Langevin equations[27] from which the Rouse model may be derived. Neigher the Rouse model nor our Monte Carlo process, however, contains any hydrodynamic flow effects, and thus our model at late stages will reproduce a coarsening behavior characteristic for solid mixtures[59] rather than for liquid mixtures.[60] As is well-known, this problem is not important during early and intermediate states of phase separation.[26]

4. Spinodal Decomposition for the Model with Repulsive Interaction between Monomers of Different Kind

Simulations have been carried out for $N = 32$ and monomer volume fractions $\phi_A = \phi_B = 0.2$ at inverse temperatures $\epsilon/k_BT = 0.2$, 0.3, 0.6, and 1.0, as well as for $N = 8$ at $\phi_A = \phi_B = 0.2$ at inverse temperatures $\epsilon/k_BT = 0.3$ and 0.6. Since the critical point occurs at[49] $\epsilon/k_BT_c \approx 0.105$ ($N = 32$) and $\epsilon/k_BT \approx 0.315$ ($N = 8$), the ratio $\chi/\chi_{crit} = T_c/T$ takes the values 1.9, 2.86, 5.72, and 9.5 ($N = 32$) and 0.95 and 1.9 ($N = 8$): thus for the case $N = 8$, $\epsilon/k_BT = 0.3$ is a quench in the critical region for T slightly above T_c, while all other quenches are rather deep quenches where χ/χ_{crit} exceeds unity distinctly.

Figure 4 shows some typical examples for the structure factor $S(q,t)$ plotted vs q at different times. Estimates for q_c are included; they were calculated from eq 8, which for the critical quench treated here ($\phi_A = \phi_B = \phi_{crit}$) reduces to $f_D(q_c^2\langle R_{gyr}^2\rangle) = \chi_{crit}/\chi$. Similarly, estimates for q_m are included which were calculated numerically from eq 4.9 or ref 20, since for our range of χ/χ_{crit} the asymptotic expressions $q_m = q_c/\sqrt{2}$ and eq 13 are not yet very accurate. It is seen that q_m predicts the position, where the *difference* $S(q,t) - S(q,0)$ develops a maximum for early times, in rough agreement with the data. On the other hand, q_c seems to have little significance: while according to the linear Cahn[28] theory $S(q_c,t) =$ constant, independent of time, no intersection occurs at early times at all; at later times, however, curves $S(q,t)$ for different values of time do intersect each other, but at the same time the maximum of $S(q,t)$ shifts to lower values of q_m as time proceeds and so does the intersection point: this behavior, which is very familiar from small-molecule liquid mixtures and metallic alloys,[4,5,26] simply reflects the onset of coarsening.

In order to perform a more meaningful comparison with the phenomenological theory of section 2, we plot $S(q,t)$ versus time t at the different q values available in our simulation (Figure 5). While eq 2 suggests that for $q < q_c$ we obtain a variation that increases exponentially with time, which implies an upward curvature of the curves shown in Figure 5, we see that there is no evidence at all for an exponential increase of intensity with time: the curves show a linear increase with time and then bend down, reflecting the immediate onset of strong nonlinear effects. This behavior is the same as that which has been observed in simulations of spinodal decomposition in metallic alloys.[39-41] In order to extract an initial rate $R(q)$ from our data, we fit a straight line to the curves in Figure 5 over the time interval $0 < t < 100$ to obtain $dS(q,t)/dt|_{t=0}$. Clearly, the choice of this time interval is somewhat arbitrary: ideally, one would like to make this time interval as short as possible, to avoid systematic errors due to the gradual onset of nonlinear effects. However, it we choose the time interval in our simulation distinctly smaller than $t < 100$, the data for the derivative $dS(q,t)/dt|_{t=0}$ get too noisy to allow a meaningful analysis. According to eqs 2 and 6, the initial derivative of the structure factor should be

$$\left.\frac{dS(q,t)}{dt}\right|_{t=0} = -2R(q)[S_T^{coll}(q) - S(q,t=0)] = q^2\Lambda(q)[1 - S(q,t=0)/S_T(q)] \quad (23)$$

which with the help of eq 3 can be rewitten as

$$\left.\frac{dS(q,t)}{dt}\right|_{t=0} = q^2\Lambda(q)\left[1 - \frac{1}{\phi_0(1-\phi_0)} + 2\chi S(q)\right] \approx q^2\Lambda(q)\left[1 - \frac{1}{\phi_0(1-\phi_0)} + 4\frac{\chi}{\chi_{crit}}\left(1 - \frac{\langle R_{gyr}^2\rangle q^2}{3}\right)\right] \quad (24)$$

For small q this hence also yields a Cahn plot $R(q^2)/q^2$

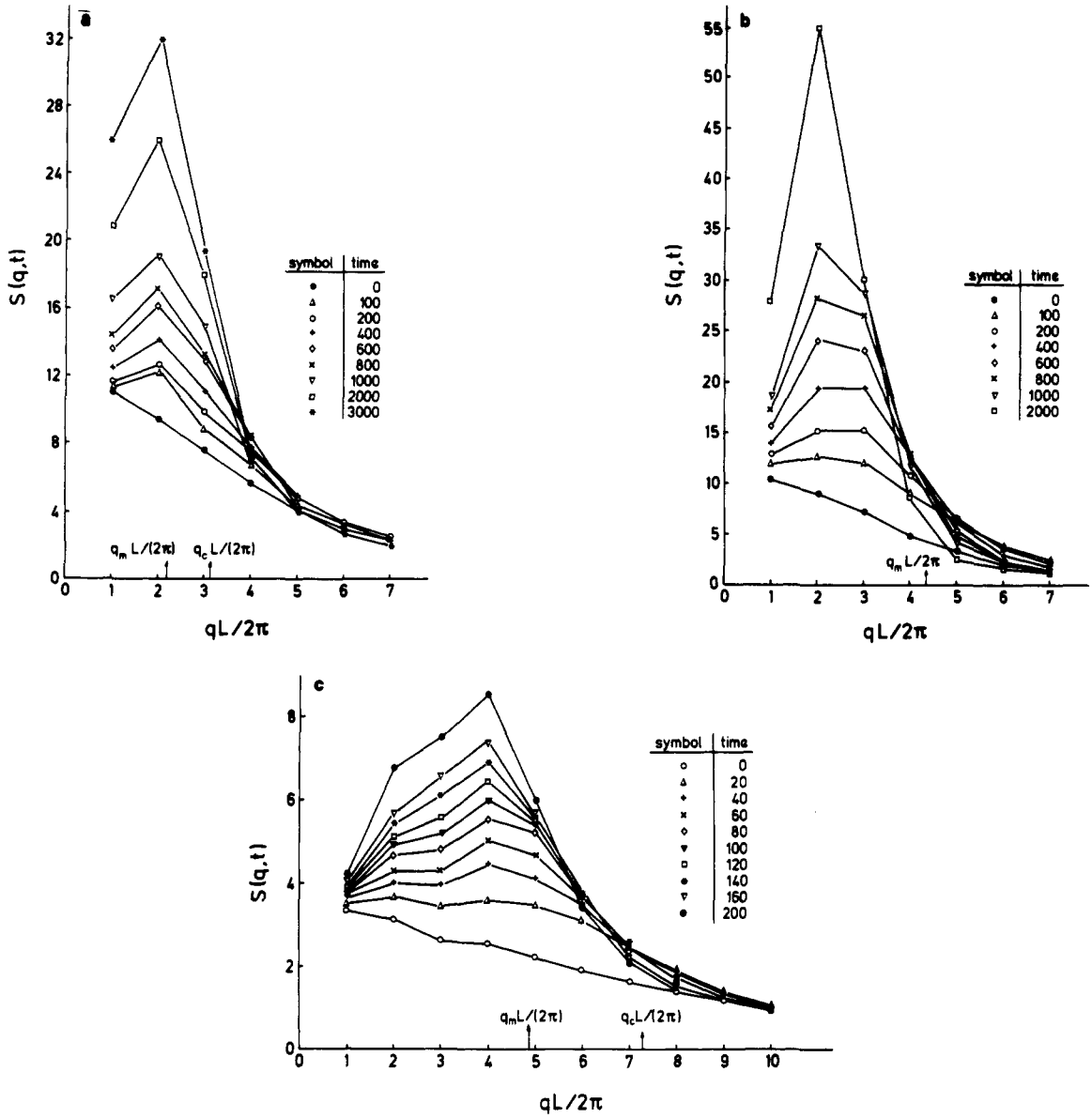

Figure 4. Collective structure function $S(q,t)$ plotted versus q at various times t after the quench from infinite temperature to the considered temperature. Case a refers to $N = 32$ and $\epsilon/k_BT = 0.2$, case b to $N = 32$ and $\epsilon/k_BT = 1$, and case c to $N = 8$ and $\epsilon/k_BT = 0.6$. The arrows show the predictions of the linearized theory of spinodal decomposition for q_m and q_c, as discussed in the text. Note that $S(q,t)$ is defined only for the discrete values $q_\nu = (2\pi/L)\nu$, $\nu = 1, 2, 3,$ and ..., characterized by the various symbols. For better visualization, these symbols are connected by straight lines in the figure. In Figure 4b $q_cL/2\pi \approx 9.2$ and hence is off-scale.

linear in q^2, for $\phi_0 = \phi_{crit} = {}^1/_2$

$$\frac{1}{q^2\Lambda(0)}\frac{dS(q,t)}{dt}\bigg|_{t=0} = 4\frac{\chi}{\chi_{crit}} - 3 - \frac{4}{3}\frac{\chi}{\chi_{crit}}\langle R_{gyr}^2\rangle q^2 \quad (25)$$

It is seen that apart from the constant $\Lambda(0)$, which can be absorbed in the time scale, the comparison between the initial slope $dS(q,t)/dt|_{t=0}$ only involves the known quantities χ/χ_{crit} and $\langle R_{gyr}^2\rangle$; no adjustable parameter whatsoever enters. This comparison between the phenomenological theory and the simulation is presented in Figure 6.

It should be noted that eq 24 is only valid for $\langle R_{gyr}^2\rangle q^2 < 1$ and most of the computer simulation results are in a regime where this inequality does not hold. An extension of the linear theory of spinodal decomposition valid in the regime $\langle R_{gyr}^2\rangle q^2 > 1$ as well has been suggested in ref 20; the result is shown in Figure 6b, suppressing a rate factor that can be absorbed in the normalization of the ordinate scale. It is seen that for large T_c/T where $q_c^2\langle R_{gyr}^2\rangle \gg 1$ there occurs pronounced curvature on the Cahn plot Figure 6b, and there is a qualitative agreement between this linearized theory and the simulation results, apart from the vicinity of q_c. However, the simulation results exhibit a pronounced curvature at all values of T_c/T studied, and a well-defined estimate of q_c can hardly be identified, while linearized theory exhibits a well-defined q_c with $q_c \to 0$ as $T_c/T \to 1$; in this limit the Cahn plot develops toward a straight line, in disagreement with the simulation data. Note that in experiments[11] linear Cahn plots were found but all these data refer to $q_c\langle R_{gyr}^2\rangle < 1$ and to much larger chain lengths.

There are essentially two reasons why one might expect that the linearized theory of spinodal decomposition cannot account for the simulations: (i) The chain lengths N are too short to satisfy the Ginzburg criterion[20] for the validity of the linearized theory. (ii) The large content of vacancies invalidates the simple versions of the theory[18-20] where the two volume fractions ϕ_A and ϕ_B of the two kinds of monomers are no independent variables since $\phi_A{}^i + \phi_B{}^i = 1$, while in our case $\phi_A{}^i + \phi_B{}^i = 1 - \phi_V{}^i = \rho^i$ also is a

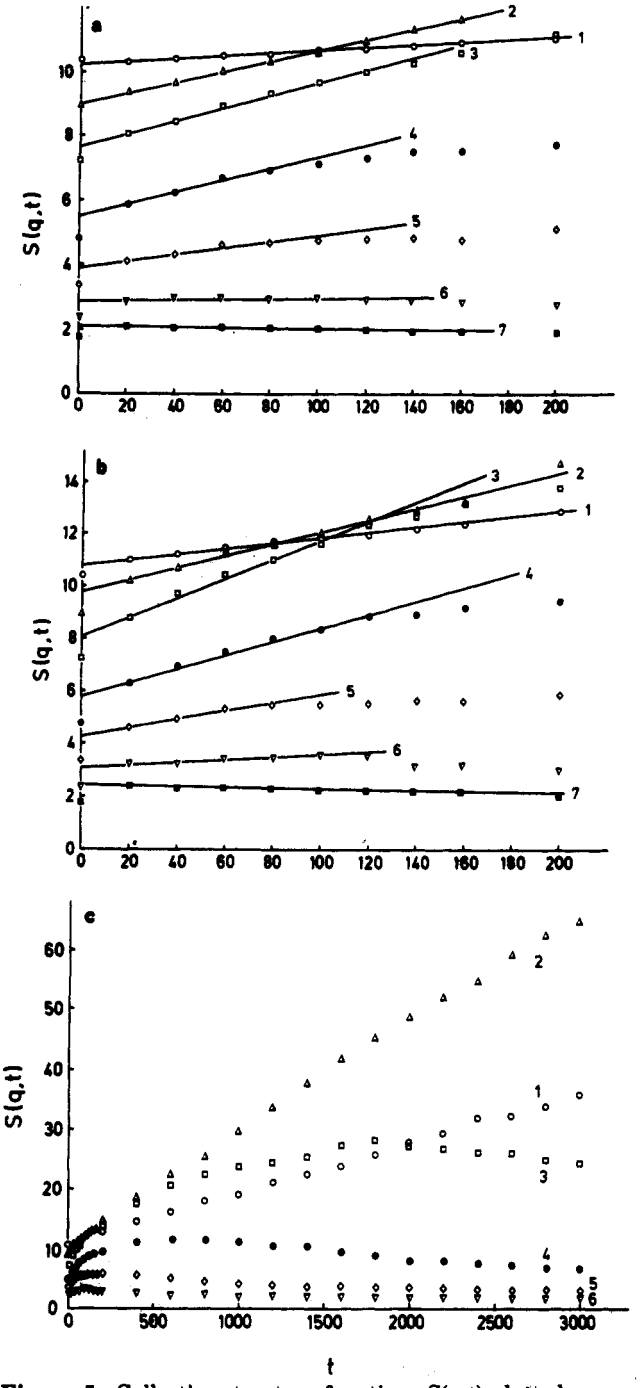

Figure 5. Collective structure functions $S(q,t)$ plotted versus time for various values of q as indicated in the figure (data are labeled by $\nu = 1, 2, 3$ related to q via $q = 2\pi\nu/L$). Case a refers to $N = 32$ and $\epsilon/k_BT = 0.3$ and cases b and c refer to $N = 32$ and $\epsilon/k_BT = 0.6$, where case b refers to early times and case c to intermediate times. The straight lines in cases a and b indicate how an effective relaxation rate, $R(q)$, can be extracted from the slope $dS(q,t)/dt$ over a time interval from $t = 0$ to $t = 100$ Monte Carlo steps.

dynamical variable which may fluctuate and couple to the fluctuations in the relative concentrations of the polymers.

In order to check for the behavior of the polymer density, ρ^i, the structure factor $S_\rho(\vec{q},t)$ (eq 21) has also been analyzed (Figure 7). It is seen that $S_\rho(\vec{q},t)$ is essentially constant in the q-range of interest and independent of time, apart from statistical fluctuations. As we shall see, this behavior is in marked contrast to our findings for the model with $\epsilon_{AA} = \epsilon_{BB} = -\epsilon$ and $\epsilon_{AB} = 0$ (section 5).

In order to study the behavior of $S(q,t)$ at intermediate times, it is convenient to analyze the time dependence of

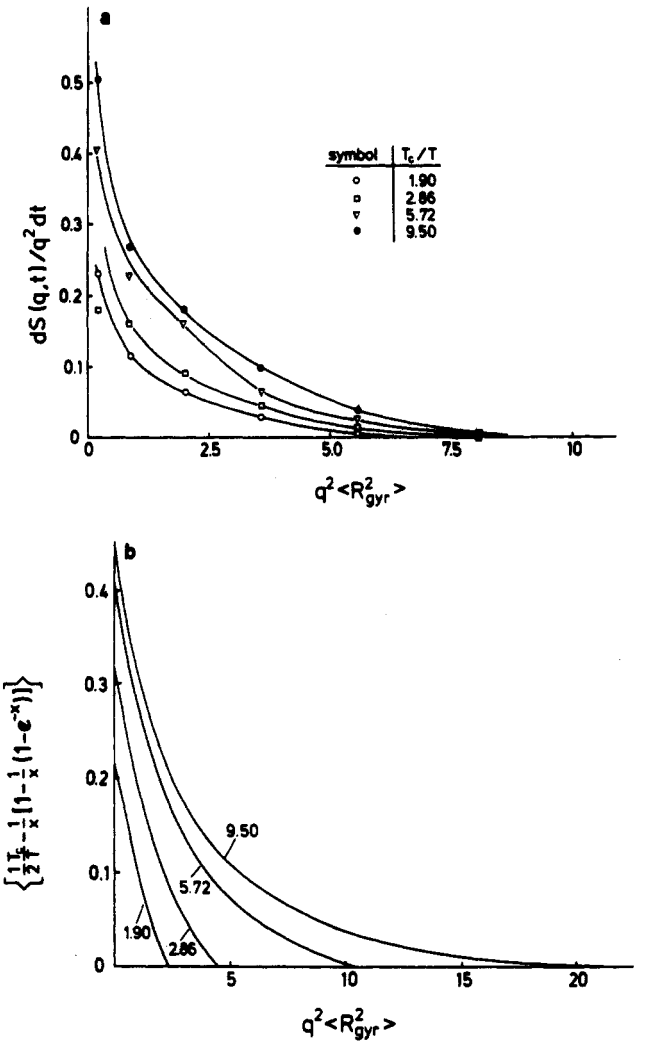

Figure 6. (a) Cahn plot $dS(q,t)/[q^2dt]$ vs q^2 obtained from the simulation data, as indicated in Figure 5 and discussed in the text. All data refer to $N = 32$. Different values of T_c/T are indicated in the figure. (b) Same as (a) but calculated from the phenomenological theory of ref 20, which leads to $dS(q,t)/[q^2dt] \sim \{(1/2)(T_c/T) - (1/x)[1 - (1/x)(1 - e^{-x})]\}$ with $x = \langle R_{gyr}^2\rangle q^2$.

the moments.

$$q_n(t) = \sum_q q^n S(q,t) / \sum_q S(q,t) \tag{26}$$

It is seen (Figure 8a) that, for times $t \lesssim 100$, $q_1(t)$ is basically time-independent. This is the time regime for which we have tried to carry out a comparison with the linearized Cahn-type theory of spinodal decomposition in Figures 4–7. At somewhat later times a decrease of $q_1(t)$ with increasing time occurs, signifying the gradual onset of coarsening. If one would try to describe this behavior in terms of a power law

$$q_1(t) \sim t^{-a} \tag{27}$$

the exponent a in the time range from $t \approx 600$ to $t \approx 3000$ would be distinctly temperature-dependent: for $\epsilon_{AB}/k_BT = 0.2$ we have $a \approx 0.12$, while for $\epsilon_{AB}/k_BT = 1.0$ we have $a \approx 0.22$, and for intermediate temperatures the exponent lies in between ($a \approx 0.15$ for $\epsilon_{AB}/k_BT = 0.3$ and $a \approx 0.18$ for $\epsilon_{AB}/k_BT = 0.6$). The occurrence of effective exponents $a(T)$ in an intermediate time range with $a(T)$ increasing with increasing quench depth has also been found experimentally.[11] It must be emphasized, however, that the asymptotic power law (eq 26) for $t \to \infty$ in our model should be $a = 1/3$, assuming that the Lifshitz–Slyozov

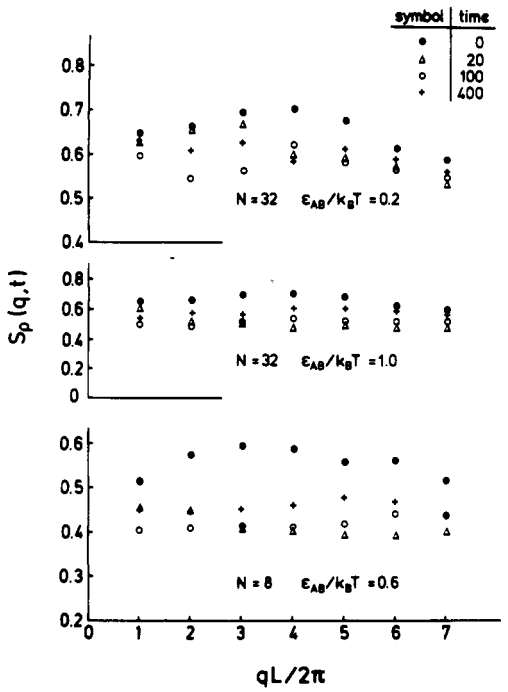

Figure 7. Collective structure function $S_\rho(q,t)$ plotted versus q at various times t after the quench from infinite temperature to the considered temperature. Cases shown correspond to the case of Figure 4.

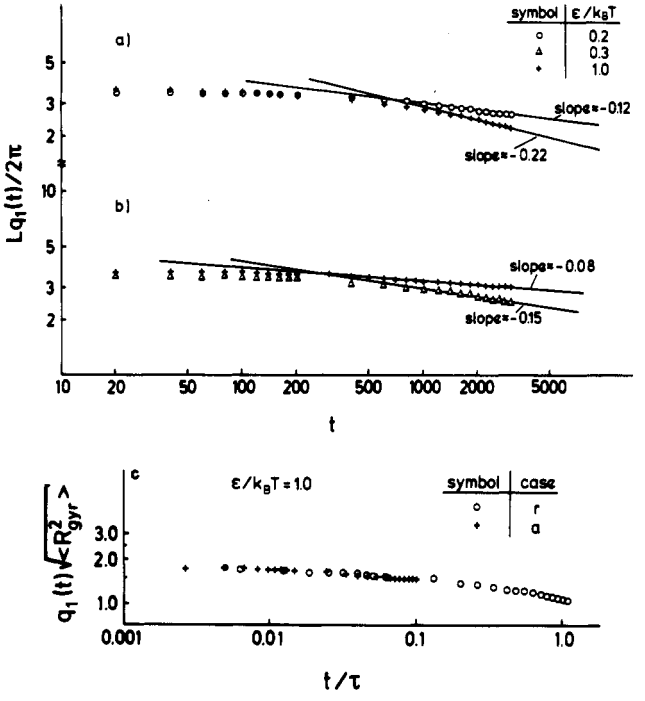

Figure 8. log–log plot of the first moment $q_1(t)$ versus time. All data refer to $N = 32$ and $\phi_A = \phi_B$. Different values of ϵ/k_BT are indicated in the figure. The numbers quoted at the straight lines indicate the effective exponent a in the relation $q_1(t) \sim t^{-a}$. Case a of the figure refers to $\epsilon = \epsilon_{AB}$ and $\epsilon_{AA} = \epsilon_{BB} = 0$, while case b refers to $\epsilon = -\epsilon_{AA} = -\epsilon_{BB}$ and $\epsilon_{AB} = 0$. Case c represents a rescaled plot of the data for $q_1(t)$ vs t at $\epsilon/k_BT = 1$ where the case $\epsilon = \epsilon_{AB}$ and $\epsilon_{AA} = \epsilon_{BB} = 0$ (repulsive interaction, denoted as "r") and the case $\epsilon = -\epsilon_{AA} = -\epsilon_{BB}$ and $\epsilon_{AB} = 0$ (attractive interaction, denoted as "a") are plotted vs a reduced time t/τ with $\tau \equiv \langle R_{gyr}^2\rangle / D_{eff}(t)$, $D_{eff}(t)$ being an effective chain self-diffusion constant, which is discussed in eq 29.

mechanism[59] of coarsening holds, while real polymer mixtures exhibit the result $a = 1$[11] proposed by Siggia.[60] As noted in the previous section, this discrepancy stems from the fact that our hopping model of polymer dynamics (Figure 2) really better corresponds to a solid polymer mixture rather than a fluid mixture, where hydrodynamic flow effects take over at late stages of the phase-separation process.[24,60] It should be noted that a detailed explanation of the effective exponents at intermediate times in Figure 8 or in experiment[11] is not known: ideas about "cluster dynamics" have led to the proposals $a = 1/6$ at low temperatures[61] and $a = 1/4$ at higher temperatures,[62] and it is believed[24] that these estimates should apply to polymer mixtures, too. However, neither experimental work[11] nor the present simulations is consistent with these predictions. We think that the behavior seen in Figure 8 should be interpreted as a gradual approach to the asymptotic universal power law describing phase separation of solid mixtures,[59] $q_1(t) \sim t^{-1/3}$, but extremely costly simulations extending to much longer times would be needed to show this.

5. Spinodal Decomposition for the Model with Attractive Interactions between Monomers of the Same Kind

Simulations were carried out for $N = 32$ and $\phi_A = \phi_B = 0.2$ at $\epsilon/k_BT = 0.3$, 0.6, and 1.0 and for $N = 32$, $\phi_A = 0.32$, and $\phi_B = 0.08$ at $\epsilon/k_BT = 0.6$. The critical point occurs at $\epsilon/k_BT_c \approx 0.0917$. Thus all data are in the regime of deep quenches.

Typical data for presented in Figures 8b, 9, and 10. While at first glance the data for $S(q,t)$ look similar to those presented in Figure 4, a closer examination reveals important distinctions: while the phase separation proceeded faster with increasing ϵ/k_BT (and hence with increasing quench depth) for $\epsilon = \epsilon_{AB}$, it is seen that for the case $\epsilon = -\epsilon_{AA} = -\epsilon_{BB}$ the phase separation proceeds faster for $\epsilon/k_BT = 0.3$ than for $\epsilon/k_BT = 1.0$. This observation also is reflected in a smaller value of the effective exponent a in the relation eq 26 (see Figure 8, lower part).

At the same time, the structure function $S_\rho(q,t)$ clearly reveals for $\epsilon/k_BT = 1.0$ also a phase separation between polymers and vacancies takes place (Figure 10b): the growing peak of $S_\rho(q,t)$ does not seem to settle down at a limiting Ornstein–Zernike function describing polymer density fluctuation correlations in a macroscopically homogeneous polymer–vacancy system

$$S_\rho(q,t\to\infty) \sim (1 + q^2\xi^2)^{-1} \qquad (28)$$

ξ being the correlation length of the polymer density fluctuations. On the other hand, for $\epsilon/k_BT = 0.3$ the results (Figure 10a) are compatible with the gradual approach toward eq 27, which would then appear as an envelope of all the curves $S_\rho(q,t)$ for finite t. In all cases, however, the behavior of $S_\rho(q,t)$ is quite distinct from the structureless behavior found in the case of repulsive interactions between unlike monomers (Figure 7). The behavior of Figures 9 and 10 demonstrates that already on the level of the linearized Cahn–Hilliard-type theory, eqs 2, 6, and 11–14 are too simple, because they consider concentration fluctuations only, and even on the level of this mean-field theory, one must consider simultaneously concentration fluctuations and polymer density fluctuations. Therefore, a comparison between the theory of section 2, and the results shown in Figures 9 and 10 is not very meaningful and has not been performed.

Figures 9c and 10c show the behavior of an off-critical quench for $\phi_A/(1 - \phi_V) = 0.8$ and $\phi_B/(1 - \phi_V) = 0.2$. It is seen that also in this case one still has an A–B phase separation by spinodal decomposition occurring, accompanied by a phase-separation polymers–vacancies. Comparing these data to results for $\phi_A = \phi_B$ taken at the same

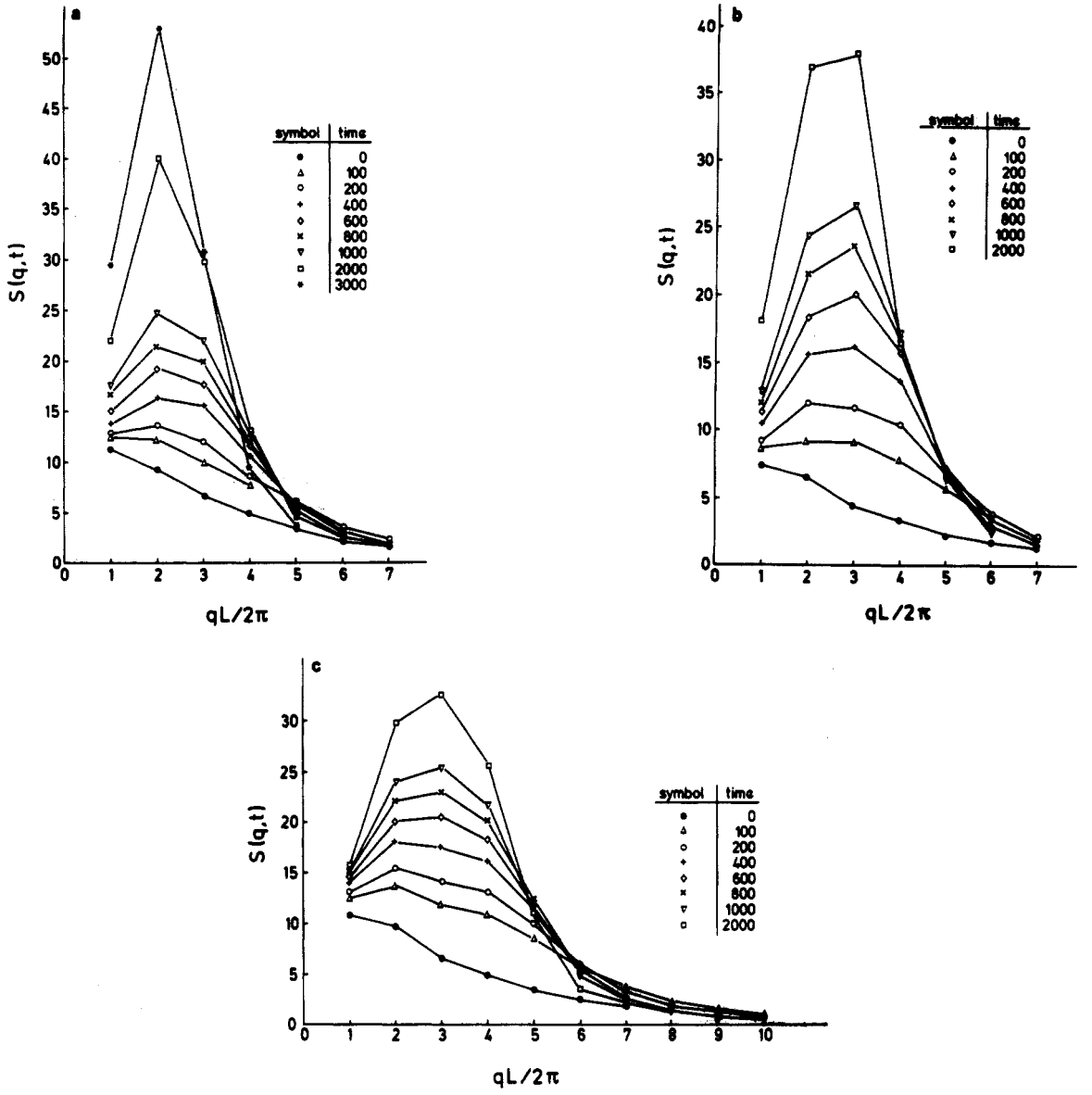

Figure 9. Collective structure function $S(q,t)$ plotted vs q at various times t after the quench from infinite temperature to the considered state. All data refer to $N = 32$ and $\epsilon_{AB} = 0$ ($\epsilon_{AA} = \epsilon_{BB} = -\epsilon$). Case a refers to $\epsilon/k_BT = 0.3$ and $\phi_A = \phi_B = 0.2$, case b refers to $\epsilon/k_BT = 1.0$ and $\phi_A = \phi_B = 0.2$, and case c refers to $\epsilon/k_BT = 0.6$, $\phi_A = 0.32$, and $\phi_B = 0.08$.

temperature $\epsilon/k_BT = 0.6$,[48] we see that the polymer–vacancy phase separation for this off-critical quench proceeds distinctly faster and the polymer–polymer phase separation proceeds distinctly slower. In fact, for still higher vacancy content a situation is conceivable where the polymer species A and B are compatible in the homogeneous phase containing the vacancies and only when the polymer–vacancy phase separation has proceeded to create a vacancy-rich phase and a polymer-rich phase; the A–B phase separation occurs in the latter.

The process of phase separation also is accompanied by a gradual change in the linear dimensions of the chains (Figure 11). While a small decrease in the chain linear dimensions also occurs for the case of the A–B repulsive interaction ($\epsilon_{AB} \neq 0$), this decrease is limited to a few percent only, even for very deep quenches. In contrast, for the case of attractive interactions between monomers of the same kind ($\epsilon_{AA} = \epsilon_{BB} = -\epsilon \neq 0$) this shrinking of the coil size is much more pronounced and also depends strongly on quench depth. For the deepest quench studied ($\epsilon/k_BT = 1.0$), this striking process has not even stopped after 3000 time steps. It is also remarkable that for shallower quenches a slight "overshooting" of this shrinking of the chains occurs. For off-critical quenches, the minority chains exhibit a more drastic contraction than the majority chains, consistent with what is found for the configurations of the chains in equilibrium blends.[54]

A useful measure of the degree of phase separation is the number $n_{AB}(t)$ of nearest-neighbor contacts between monomers of different kinds A and B per chain (Figure 12). In the case where $\epsilon = \epsilon_{AB}$ this quantity simply is related to the internal energy of the chains. For this quantity we also expect a power law decay

$$n_{AB}(t) - n_{AB}(\infty) \sim t^{-b} \tag{29}$$

where the exponent b at very late times also is expected to have a value consistent with Lifshitz–Slyozov theory, $b = 1/3$. Since for the very deep quenches considered in Figure 12, the final equilibrium value of contacts $n_{AB}(\infty)$ in a fully phase-separated state is negligibly small; since the solubility of the A-rich phase for B chains then is extremely small and vice versa, we have not subtracted $n_{AB}(\infty)$ in Figure 12. Nevertheless, it is seen that in the time regime from $t \approx 300$ to $t \approx 3000$ in Figure 12 the effective exponent b^{eff} in the power law eq 28, which shows

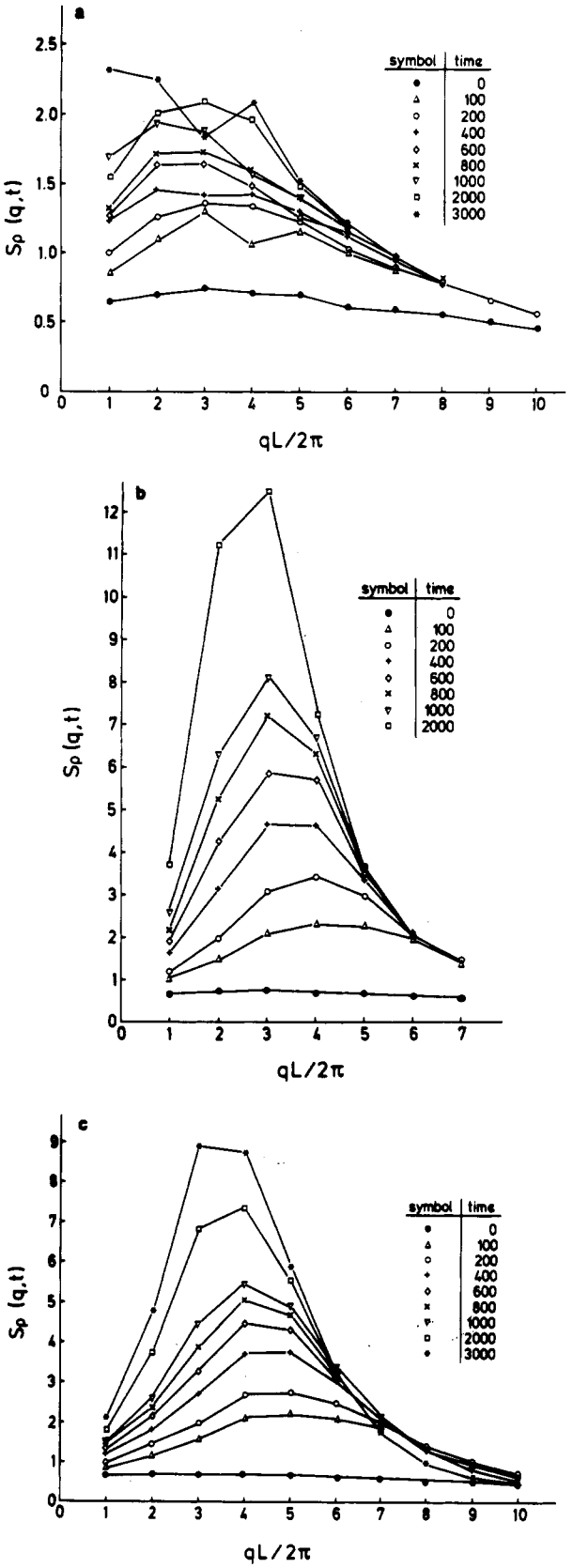

Figure 10. Collective structure function $S_\rho(q,t)$ describing the polymer density fluctuations plotted vs q at various times t after the quench. Cases shown correspond to those of Figure 9.

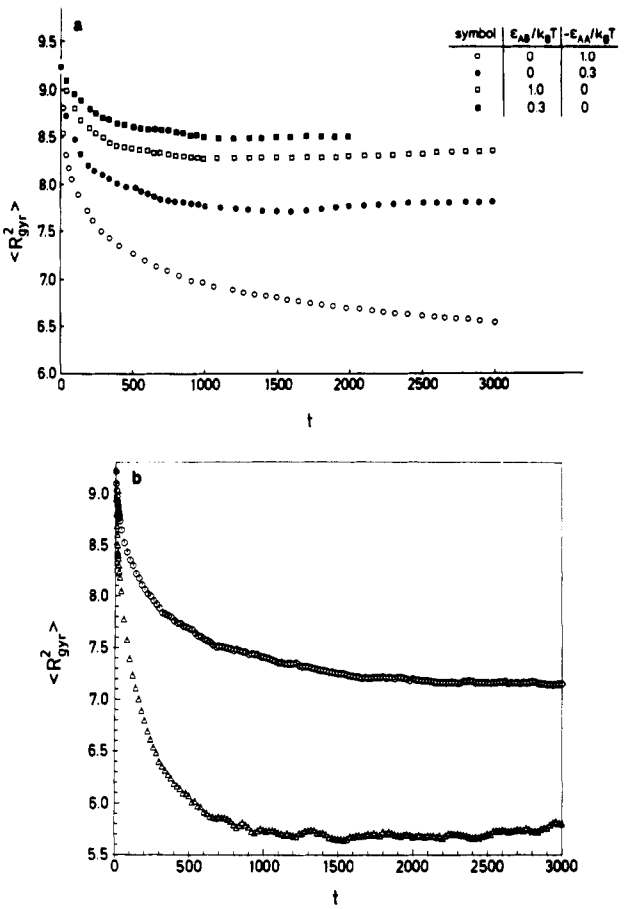

Figure 11. Gyration radius plotted vs time for $\phi_A = \phi_B = 0.2$ and various choices of the energy parameters (a) and for $\phi_A = 0.32$, $\phi_B = 0.08$, and $\epsilon/k_BT = 0.6$ ($\epsilon_{AA} = \epsilon_{BB} = -\epsilon$), case (b). In the latter case triangles denote the mean-square gyration radius of the minority component and octagons the mean-square gyration radius of the majority component.

up in the plot of Figure 12 as the slope of the curve, even may exceed the asymptotic value (e.g., for $\epsilon/k_BT = 1.0$ in case a and for $\epsilon/k_BT = 0.6$ in case b), while the effective exponent in the relation $q_1(t)$ vs t (Figure 8) in the corresponding cases is much smaller than the asymptotic value. Clearly, the asymptotic regime of late times where we expect that $a = b = 1/3$ (eqs 26 and 28) has not been reached by our simulations. Note that for $\epsilon/k_BT = 1$ one can clearly distinguish two different physical phenomena: at early times ($t \lesssim 200$), a rather strong chain contraction occurs (Figure 11), and therefore there is a rather strong initial decrease in the number of (unfavorable) AB contacts due to the formation of (favorable!) AA and BB self-contacts. Therefore, $n_{AB}(t)$ for $\epsilon/k_BT = 1$ lies below $n_{AB}(t)$ for $\epsilon/k_BT = 0.6$ in Figure 12b. The later stage, however, requires interdiffusion of chains in order to form more extended A-rich and B-rich regions: this interdiffusion proceeds much faster (see Figure 14 below) for $\epsilon/k_BT = 0.6$ than for $\epsilon/k_BT = 1.0$, and therefore for these later times ($t \gtrsim 600$) the data for $\epsilon/k_BT = 1.0$ lie above those for $\epsilon/k_BT = 0.6$ in Figure 12b. We think that this interpenetration of pairs of chains, which at $t = 0$ have been both self-avoiding and mutually avoiding, is responsible for the strong decrease of $n_{AB}(t)$ seen in Figure 12 for later times.

While the number of contacts $n_{AB}(t)$ between monomers of different kinds is a decreasing function of time, the number of self-contacts in a chain increases with time (Figure 13). This increase in the number of self-contacts reflects the decrease of the coil size (Figure 11); of course, the more compact a chain configuration becomes, the more self-contacts are expected.

This change of the coil configuration in deep quenches also has an effect on the mobility of the coils. This is seen when we define an effective self-diffusion coefficient of

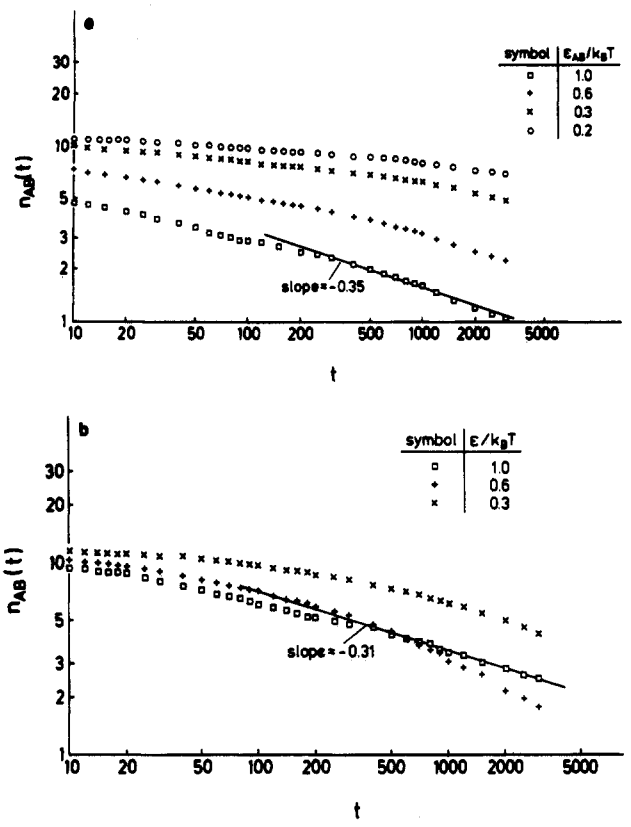

Figure 12. log–log plot of the number $n_{AB}(t)$ of contacts between monomers of a different kind per chain plotted vs time, for $N = 32$, $\phi_A = \phi_B = 0.2$, $\epsilon = \epsilon_{AB}$, and $\epsilon_{AA} = \epsilon_{BB} = 0$ (a) and for $\epsilon_{AB} = 0$ and $\epsilon_{AA} = \epsilon_{BB} = -\epsilon$ (b).

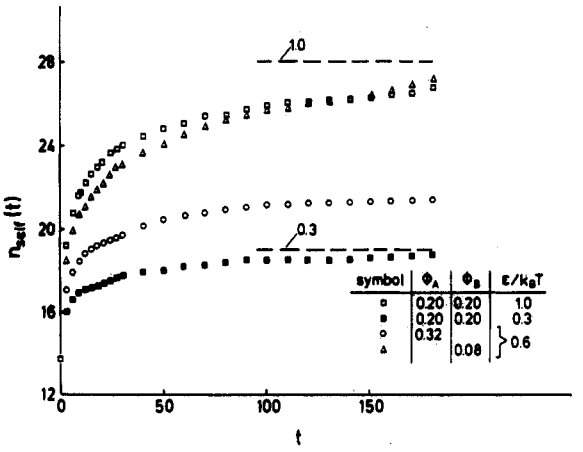

Figure 13. Number of self-contacts between monomers in a chain for $N = 32$ plotted vs time. All data refer to $\epsilon_{AA} = \epsilon_{BB} = -\epsilon$ and $\epsilon_{AB} = 0$. For two cases the "asymptotic" value $n_c^{self}(t\to\infty)$ is shown by a dashed horizontal straight line. This value is estimated from the time regime from $t = 1000$ to $t = 3000$ time steps.

the coils as

$$D_{eff}^{A,B}(t) = \frac{\langle[\vec{r}_{CG}(t) - \vec{r}_{CG}(t-\Delta t)]^2\rangle_{A,B}}{6\Delta t} \qquad (30)$$

where $\vec{r}_{CG}(t)$ is the center of gravity of an A polymer (or B polymer, respectively) at time t after the quench, and the average in eq 29 is taken over all samples and over all polymers of the considered types A and B (for $\phi_A = \phi_B$, both polymer species are equivalent and are hence averaged over). The time interval, Δt, in eq 29 should, in principle, be larger than the chain relaxation time; for practical reasons we have limited it rather to $\Delta t = 20$ MCS.

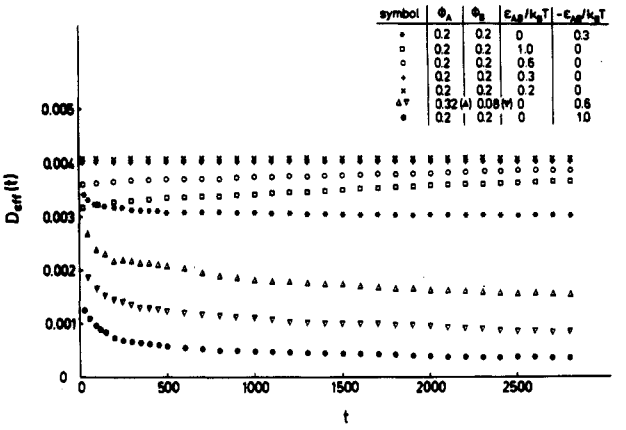

Figure 14. Effective self-diffusion constant, $D_{eff}(t)$, as a function of time after the quench for $N = 32$ and various choices of interaction parameters as indicated in the figure.

From Figure 14 it is seen that for repulsive interactions ($\epsilon_{AB} > 0$, $\epsilon_{AA} = \epsilon_{BB} = 0$) the effective diffusion constant slightly increases as the time after the quench proceeds, for deep quenches, while for shallow quenches $D_{eff}(t)$ is independent of time. In addition, the dependence of $D_{eff}(t)$ on temperature is not very large. For the case of attractive interactions, however, this is not true: while for not very deep quenches $D_{eff}(t)$ is similar in magnitude to the repulsive case and $D_{eff}(t)$ always is a decreasing function of time, for deep quenches $D_{eff}(t)$ is 1 order of magnitude smaller than that in the case of repulsive interactions. A remarkable asymmetry arises also for the off-critical quench: for $\epsilon/k_BT = 0.6$, the diffusion constant of the minority component then is about a factor of 2 smaller than that of the majority component!

Since the self-diffusion process of the chains sets the time scale for the kinetics of phase separation as well, it is useful to convert our results to a *dimensionless time scale* t/τ, where τ is a characteristic time of a polymer chain needed to diffuse over a distance comparable to its linear dimension. Hence we define τ as

$$\tau = \langle R_{gyr}^2\rangle / D_{eff}(t) \qquad (31)$$

Note that in this definition τ itself depends on the time t after the quench, of course. In eq 30, we have used the chain dimension for $\epsilon/k_BT = 0$ as quoted in eq 19 for simplicity—alternatively, we could have used the time-dependent radii shown in Figure 11 for this data reduction as well. Figure 8c contains the results for $q_1(t)$ at $\epsilon/k_BT = 1.0$ plotted in dimensionless form. This type of plot involves dimensionless quantities only, which in principle also would be accessible in experimental work as well. Two conclusions emerge from this plot: (i) The Monte Carlo results all belong to the regime $t/\tau < 10$, i.e., the regime of rather early stages, since chains have not yet had enough time to diffuse over a large distance. (ii) The distinction between Figure 8a (repulsive interaction) and Figure 8b (attractive interaction) disappears completely in the scaled plot: it simply was due to the fact that for attractive interactions the diffusion constant is so much slower that only very early stages of the phase-separation process could be resolved ($t/\tau < 1$).

6. Conclusions

In this paper we have presented rather extensive computer simulation studies of spinodal decomposition of symmetrical polymer mixtures, both for critical quenches ($\phi_A = \phi_B$) and for a quench at strongly off-critical composition [$\phi_A/(1 - \phi_V) = 0.8$ and $\phi_B/(1 - \phi_V) = 0.2$],

considering both the case of repulsive interaction between unlike monomers and the case of attractive interactions between monomers of the same kind. Our model contains many vacancies ($\phi_V = 0.6$) and thus is in some respects a model of a dense solution of two polymers in a common solvent rather than a model of a mixed polymer melt. Therefore both cases are not at all equivalent.

The model studied is a dynamic version of the Flory–Huggins lattice model. In this respect it differs significantly from a recent study,[67] where the continuum Flory–Huggins free energy density augmented with square gradient terms[20] was used as a starting point for simulations using a numerical Langevin equation approach. In our previous work[49] on the static properties of the Flory–Huggins lattice model, we have shown that the Flory–Huggins free energy, which results from the lattice model only via drastic approximations, is a rather inaccurate description of the lattice model. In addition, this approach used in ref 67 is applicable only in the long-wavelength limit; i.e., the wavevectors of interest are restricted to the range $q(\langle R_{gyr}^2\rangle)^{1/2} < 1$: as pointed out in ref 20, the square gradient approximation even within the framework of mean-field theory is valid only for this long-wavelength limit. Since in our case $q_1(t)(\langle R_{gyr}^2\rangle)^{1/2} \gtrsim 1$, (see Figure 8c), we are concerned with a parameter regime that could not be treated by the approach of ref 67.

Our results can be summarized as follows: the collective structure factor during the initial stages (Figures 4 and 9) starts out with the single-chain structure factor, since our starting condition is a completely random mixture of A and B chains consistent with the chosen volume fraction, and then develops a peak at a position $q_m(t)$, which is practically independent of time for $t < \tau$, τ being a characteristic time for chain self-diffusion (Figure 8c). This initial position is predicted correctly within about 50% by the phenomenological theory of ref 20, which is an extension of the Cahn–Hilliard-type theory[18,19,28] to larger wavevectors by means of the "random-phase approximation".[52] Note that this comparison of wavevectors between theory and simulation does not involve any adjustable parameter whatsoever, since wavevectors are measured in units of the gyration radius $(\langle R_{gyr}^2\rangle)^{1/2}$, which is also known in the simulation, see eq 19, and temperature T is measured in units of T_c, which is also known,[49] and we invoke the relation $\chi_c/\chi = T/T_c$ valid in Flory–Huggins theory. This fact that the phenomenological theory can predict successfully the correct wavelength scale $q_m(t=0)$ where the phase separation starts is also true for experiments,[1,2,4,10,11,15] which typically refer to polymer mixtures with much longer chain lengths and comparably shallow quenches. Our results suggest that for predicting $q_m(t=0)$ in polymer mixtures the phenomenological theory can still be used under rather extreme conditions, where all other features of this theory is no longer true. This becomes already evident from a consideration of the growth of $S(q,t)$ during the initial stages (Figure 5): rather than the predicted exponential growth,[18–20] which indeed is observed experimentally for very long chains,[1–11] we only find a growth linear with time or even slower, as for mixtures of small molecules[26] and corresponding simulations.[39,40] The corresponding "Cahn plot" of the growth rate (Figure 6a) is therefore always distinctly nonlinear, unlike some of the experiments.[11] It should be emphasized, however, that for deep quenches ($\chi_c/\chi \ll 1$) where $q_m(t=0)(\langle R_{gyr}^2\rangle)^{1/2} > 1$ a pronounced curvature of the Cahn plot already results from the phenomenological theory of ref 20; see Figure 6b. Note that the comparison between parts a and b of Figure 6 involves only a scale factor of the ordinate scale as an adjustable parameter; therefore, the general similarity of these plots is interesting. Note, however, that the simulation *never* yields a clear-cut value of the critical wavevector, q_c, unlike the phenomenological theory (Figure 6b). This discrepancy must be expected, of course, since the linearization approximation on which ref 20 is based clearly does not hold well, since otherwise we would observe the exponential growth of $S(q,t)$ with times.[20]

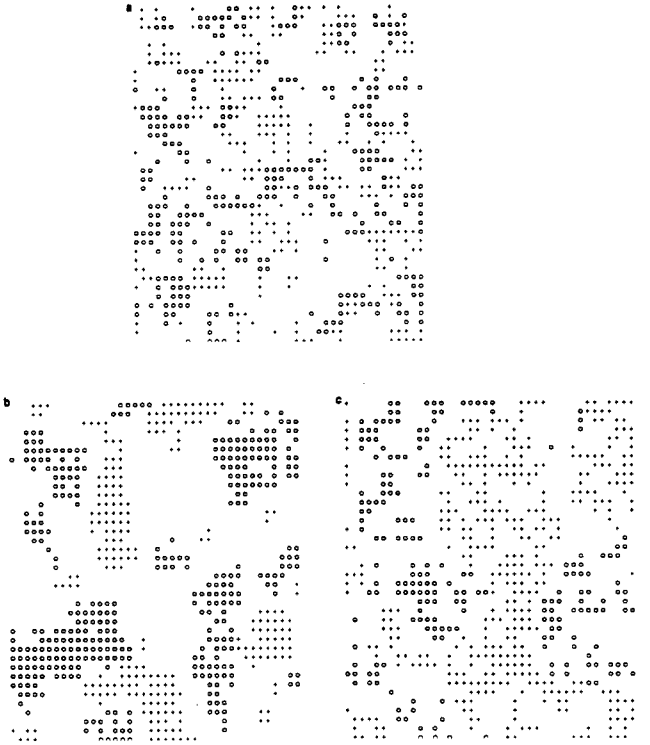

Figure 15. Snapshot picture of one 40 × 40 plane of the 40 × 40 × 40 system with $N = 32$ and $\epsilon/k_BT = 0.6$, at time $t = 0$ (a) and at time $t = 3000$ MCS/site (b and c). Case b refers to attractive interactions $\epsilon_{AA} = \epsilon_{BB} = -\epsilon$ and $\epsilon_{AB} = 0$, while case c refers to repulsive interactions, $\epsilon_{AA} = \epsilon_{BB} = 0$ and $\epsilon_{AB} = \epsilon$. Monomers of kind A are represented by + and monomers of kind B by 0; vacancies are not shown.

In our model, the case of repulsive interactions between unlike monomers ($\epsilon = \epsilon_{AB}$ and $\epsilon_{AA} = \epsilon_{BB} = 0$) and the case between attractive interactions between monomers of the same kind ($\epsilon_{AB} = 0$ and $\epsilon_{AA} = \epsilon_{BB} = 0$) behave rather differently: In the former case, the vacancies stay distributed rather randomly throughout the quench, as shown by the "flat" behavior of the structure factor $S_\rho(q,t)$ as a function of q (Figure 7). In the latter case, for shallow quenches the structure factor $S_\rho(q,t)$ probably develops toward an Ornstein–Zernike function (Figure 10a), where the correlation length, ξ (eq 27), probably is of the same order as the gyration radius: this means that there does occur a significant "expelling" of vacancies from the chains. This feature also shows up in a significant chain contraction (Figure 11a), while in the repulsive interaction case ($\epsilon_{AB} = \epsilon$), only a small contraction of chain results, even for very deep quenches. The deep quench for attractive interactions between monomers, on the other hand, is characterized by simultaneous polymer–polymer unmixing (Figure 9b) and polymer–vacancy unmixing (Figure 10b). For a strongly off-critical case, where the volume fraction of B is nearly dilute ($\phi_B = 0.08$), the polymer–vacancy separation (Figure 10c) is a particularly pronounced phenomenon. This polymer–vacancy segregation also is evident from a direct inspection of "snapshot pictures" of the configurations (Figure 15).

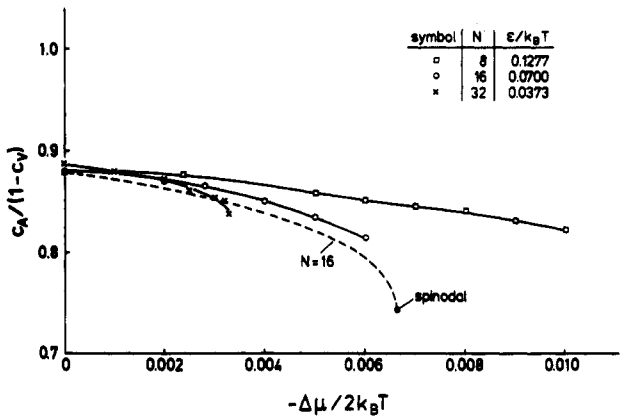

Figure 16. Metastable branches of a polymer mixture with $\phi_V = 0.2$ and three choices of chain length N and temperature as indicated. The broken curve shows the corresponding Flory–Huggins mean-field equation of state for $N = 16$, ending in a spinodal singularity.

The "collapse" of the polymer chain for the case of deep quenches with attractive interactions (Figure 11a,b) leads also to a pronounced decrease in the number of A–B nearest-neighbor contacts between monomers (Figure 12b) and a pronounced increase in the number of A–A (B–B) self-contacts (Figure 13). It would be very interesting to look for such effects in experimental studies on the phase separation of polymer mixtures in the presence of a common solvent. Such studies would be a rather clear proof of whether the effective interaction is predominantly attractive (as modeled by $\epsilon_{AA} = \epsilon_{BB} = -\epsilon$ here) or repulsive ($\epsilon = \epsilon_{AB}$). It is also interesting that this change in chain conformation leads to a pronounced decrease in the self-diffusion constant of chains (Figure 14). For the off-critical quench, the decrease of the radius is much more pronounced for the minority component (Figure 11b) than for the majority component, and then the self-diffusion constant for chains of the minority component is about a factor of 2 smaller than for chains of the majority component (Figure 14), although in the absence of interactions our model is perfectly symmetric, and both types of chains have the same self-diffusion constant. In a real polymer mixture, where there is already some asymmetry arising from the different chemical structure of the two constituents, the asymmetry due to off-critical concentration and resulting different chain conformation superimposes of the "natural" (chemically based) asymmetry, and then the proper interpretation of data may be quite difficult.

Since our model throws out hydrodynamic interactions and the resulting unmixing mechanisms based on hydrodynamic viscous flow by construction, it makes little sense to attempt a study of the scaling behavior occurring[1-5] at late stages ($q_m(t) \ll q_m(0)$) of phase separation. But it is interesting to focus on the onset of coarsening, where $q_m(t)/q_m(0) \gtrsim 1/2$, where in the relation q_m vs t or q_1 vs t, an analysis in terms of effective power laws $q_1(t) \sim t^{-a}$ is quite common.[5,10,24,26,39,40,61] We do not obtain any clear evidence for the result $a = 1/6$ from the cluster-diffusion-coagulation mechanism,[24,61] but rather the effective exponent a seems to depend on quench depth, as found in simulations on Ising models.[26,39,40] In the repulsive case, we see an increase of this effective exponent with increasing quench depth (Figure 8a), qualitatively similar as a recent experiment:[11] however, the latter obtains similar values for a for much smaller quench depths than studied in the simulation. We feel that the behavior seen in Figure 8a is a gradual crossover toward the universal Lifshitz–Slyosov[59] coarsening law $q_1(t) \sim t^{-1/3}$ valid in the late stages of all solid mixtures. Due to our choice of local motions on the lattice, corresponding to a Rouse-like motion of single chains, the model corresponds to unmixing of a solid mixture rather than a fluid mixture, during the late stages. Due to the high viscosity of polymer melts, their finite (rather than infinite) viscosity plays no role during the early and intermediate stages of phase separation.

While for our model a spinodal curve can be constructed by extrapolation (Figure 3), it does not play any special role for phase separation: the results in Figure 9c are for an off-critical quench, where q_m now should be significantly reduced in comparison with Figure 9a,b due to the proximity of the spinodal curve (which occurs for $\phi_A/(1 - \phi_V) \simeq 0.96$ at $\epsilon/k_BT = 0.6$ in the attractive energy case where $\epsilon/k_BT_c = 0.0925$[49]). However, $q_m(t<\tau)$ in Figure 9c is roughly at the same position as in the symmetric quench case (cf. also Figure 1a of ref 48). Similarly, when homogeneous metastable one-phase states are studied (cf. Figure 16 and the Appendix), no sign of the singularity at the spinodal curve is detected either. While the regime over which the spinodal singularity is rounded off should become small (of order $N^{-1/3}$ for large N[20]), our chains clearly are too short to see this. Clearly, an extension of the present simulations to much larger chain length would be very desirable, as well as systematic studies for various vacancy concentrations. All these studies would require substantial efforts of computing time and hence are not easily feasible at the moment. We do hope that the present simulations will stimulate corresponding experimental work in the regime of strong incompatibility, $\chi/\chi_{crit} \gg 1$, which has not been investigated systematically so far. Unlike the opposite case, where $\chi/\chi_{crit} - 1 \lesssim 1$ and hence $q_m(t)(\langle R_{gyr}^2\rangle)^{1/2} < 1$ from the beginning and the behavior is qualitatively the same as for mixtures of small molecules since the wavelengths of interest are larger than the size of a coil, in the regime $\chi/\chi_{crit} \gg 1$ where $q_m(0)(\langle R_{gyr}^2\rangle)^{1/2} > 1$, a rather different behavior occurs even on the simplified level of the linearized theory (Figure 6b).

Acknowledgment. A.S. thanks the Max Planck Institut für Polymerforschung, Mainz, for financial support. K.B. is grateful to C. C. Han, T. Hashimoto, D. W. Heermann, J. S. Higgins, K. Kremer, and P. Wiltzius for stimulating interactions.

Appendix: Simulation of Homogeneous Metastable States for Polymer Mixtures

In Figures 1 and 3, the miscibility gap has been divided into two parts by the spinodal curve, namely the metastable region and the unstable region. While it is known that in general this distinction is not sharp and the singular behavior associated with the spinodal curve is an artifact of mean-field approximations,[5,26] in polymer mixtures it is known that a spinodal curve does become well-defined in the limit chain length $N \to \infty$,[20,21] and for long chains the lifetime of metastable states becomes extremely large since the prefactor of the free energy barrier against homogeneous nucleation diverges as $N^{1/2}$ for $N \to \infty$ (in $d = 3$ space dimensions).[20,21]

Now it is not easy to distinguish this behavior from a study of the collective structure function $S(q,t)$—even in the metastable regime we expect a behavior in the early stages rather similar to that in Figures 4 and 9—only for late stages the growth of $S(q,t)$ stops at an "envelope function" $S(q,\infty) = S(0)/[1 + q^2\xi_{MS}^2]$, where ξ_{MS} is the correlation length for concentration fluctuations in the

metastable state (see Binder et al.[63] for an explicit calculation that shows this fact).

Thus from the computational point of view it is much more convenient to study the hypothetical metastable one-phase states in the two-phase coexistence region by a direct calculation in the grand-canonical ensemble of the polymer mixture. In this ensemble, thermal equilibrium is considered at fixed temperature T and fixed chemical potential difference $\Delta\mu = \mu_A - \mu_B$ between the monomers. That is, the simulation takes place in contact with a reservoir of chains such that an A chain is removed from the lattice toward the reservoir and replaced by a B chain from the reservoir (in an identical configuration), and vice versa. These A $\leftrightarrow$ B interchanges occur in addition to the standard motions (shown in Figure 2) to relax the chain configurations. This technique has been used extensively for an analysis of the static thermodynamic properties of our model polymer mixtures.[49,50] The concentrations c_A and c_B are then simply obtained from sampling the numbers n_A and n_B of A chains (B chains) in the system during the simulation.

Metastable states now are studied with this technique as follows: we first equilibrate the system at the two-phase coexistence curve (for $\Delta\mu = 0$), starting the simulation in a state where all chains are A chains. Then the system relaxes rather quickly to the A-rich branch of the coexistence curve. In principle, in a finite box there is also a nonzero probability that the system jumps over to the B-rich branch, since in finite systems there is no spontaneously broken symmetry.[64] In practice, this jumping between the two branches of the coexistence curve for $\Delta\mu = 0$ occurs for $T \ll T_c$ only after extremely long runs and hence does not need to be taken into account.

Now such an equilibrated A-rich state at the coexistence curve is suddenly exposed to a negative value of $\Delta\mu$: now the stable equilibrium state is a B-rich state beyond the other branch of the coexistence curve. However, in order to reach this state from the initial A-rich state, a nucleation event where a B-rich droplet is formed is required, and if the nucleation barriers are high enough, this nucleation will not occur during the simulation time, and rather one will observe the relaxation into a metastable A-rich state in which the system persists throughout the simulation.

This technique has first been used for Ising models,[65,66] and Figure 16 shows that it works for our model of polymer mixtures, too: for three chain lengths the concentration of the metastable state is shown as a function of the chemical potential difference, $\Delta\mu$. The temperatures have been adjusted such that for $\Delta\mu = 0$ we had $\phi_A/(1-\phi_V) = 0.88$ for $N = 8$ and 16 while for $N = 32$ the choice of temperature rather yielded $\phi_A/(1-\phi_V) = 0.89$. Box sizes used ranged from 16^3 to 24^3, with the smaller size being used only for $N = 8$ and $N = 16$. These metastable branches shown in Figure 16 typically end without any visible singularity of the derivative $\partial(\phi_A)/\partial(\Delta\mu)$, because then nucleation barriers are already low enough so that nucleation toward the stable phase already would occur during the course of the simulation, if we either go somewhat deeper into the metastable region or run the simulation significantly longer at the last point shown. In this sense, the apparent limit of metastability encountered in the simulation is not completely sharply defined but depends on the observation time of the simulation! We have chosen our simulation times just large enough in order that the statistical error of the results shown in Figure 16 is about as large as the size of the symbols shown; if we would use much shorter runs we could go a little bit deeper into the metastable region but at the expense of larger statistical errors, and hence no well-defined metastable states would result.

This heuristic procedure to define metastable states is compared to mean-field predictions as follows: in terms of the "order parameter" m of the transition, related to the volume fraction ϕ_A as $m = 2[\phi_A/(1-\phi_V)] - 1$, the Flory–Huggins equation of state for a symmetric polymer mixture can be written as[49,51]

$$\frac{N\Delta\mu}{k_BT} = \ln\frac{1+m}{1-m} - mN\chi_{eff} \tag{32}$$

where χ_{eff} is an effective enthalpy parameter responsible for phase separation. Of course, it is a big problem to give this parameter a precise meaning in the context of our simulations: there is no straightforward relation between χ_{eff} and ϵ/k_BT.[49,50] In the present context, we avoid this problem, adjusting χ_{eff} such that for $\Delta\mu = 0$ the actual value of m (as observed by our simulation) is reproduced. This value of χ_{eff}, namely $N\chi_{eff} \approx 2.6216$ for $\phi_A/(1-\phi_V) = 0.88$, is used to evaluate $\Delta\mu$ as function of m from eq A1 and this yields the broken line included in eq 15. The concentration at the singular end point (spinodal) of this curve can be obtained directly[20]

$$m_{sp} = (1 - T/T_c)^{1/2} = (1 - \chi_c/\chi_{eff})^{1/2} \approx 0.4869$$
$$\frac{\phi_A^{sp}}{1-\phi_V} = (1 + m_{sp})/2 \approx 0.743 \tag{33}$$

where we have used the standard result $N\chi_c = 2$ for symmetric polymer mixtures.[51,52] It is seen that although the value of $\Delta\mu$ at the actual limit of metastability observed in the simulation ($\Delta\mu/(2k_BT) \approx -0.006$ for $N = 16$) is not much smaller (in absolute magnitude) than the mean-field value at the spinodal ($\Delta\mu^{sp}/(2k_BT) \approx -0.00664$), the associate concentration difference relative to the coexistence curve $(\phi_A^{coex} - \phi_A)/(1-\phi_V) \approx 0.065$ is much smaller than the mean-field result, $(\phi_A^{coex} - \phi_A^{sp})/(1-\phi_V) \approx 0.137$: in the (ϕ_A, T) space Flory–Huggins theory overestimates the stability regime of metastable states by a factor of 2, although in $(\Delta\mu, T)$ space it overestimates the extent of the metastable region only by about 10%. A similar behavior has also been established for the Ising model.[66] Again the conclusion is that much longer chains are needed to see the predicted validity of the Flory–Huggins spinodal singularity.[20]

References and Notes

(1) Hashimoto, T. In *Current Topics in Polymer Science*, Ottenbrite, R. M., Utracki, L. A., Inoue, S., Eds.; Hanser: Munich, Vienna, and New York, 1987; Vol. II, p 199.
(2) Nose, T. *Phase Transitions* **1987**, *8*, 245.
(3) Binder, K. *Colloid Polym. Sci.* **1987**, *265*, 273.
(4) Komura, S., Furukawa, H., Eds. *Dynamics of Ordering Processes in Condensed Matter*; Plenum: New York, 1988.
(5) Binder, K. In *Materials Science and Technology, Vol. 5: Phase Transformations in Materials*; Haasen, P., Ed.; VCH Verlagsgesellschaft: Weinheim, Germany, in press.
(6) Snyder, H. L.; Meakin, P.; Reich, R. *Macromolecules* **1983**, *16*, 757.
(7) Okada, N.; Han, C. C. *J. Chem. Phys.* **1986**, *85*, 5317.
(8) Hashimoto, T.; Izumitani, T. *J. Chem. Phys.* **1985**, *83*, 3694.
(9) Sato, T.; Han, C. C. *J. Chem. Phys.* **1988**, *88*, 2057.
(10) Wiltzius, P.; Bates, F. S.; Heffner, W. R. *Phys. Rev. Lett.* **1988**, *60*, 1538.
(11) Bates, F. S.; Wiltzius, P. *J. Chem. Phys.* **1989**, *91*, 3258.
(12) Schwahn, D.; Yee-Madeira, H. *Colloid Polym. Sci.* **1987**, *265*, 867.
(13) Schwahn, D.; Springer, T.; Mortensen, K.; Yee-Madeira, H. Reference 4, p 445.
(14) Schwahn, D.; Springer, T.; Yee-Madeira, H.; Mortensen, K. In *Springer Proceedings in Physics*; Springer: Berlin, Heidelberg, and New York, 1988; Vol. 29, p 296.
(15) Meier, H.; Strobl, G. R. *Macromolecules* **1987**, *20*, 649.

(16) Inaba, N.; Sato, K.; Suzuki, S.; Hashimoto, T. *Macromolecules* **1986**, *19*, 1690; *Ibid.* **1988**, *21*, 407.
(17) Hashimoto, T.; Takenaka, M.; Jinnai, H. *Polym. Commun.* **1989**, *30*, 177.
(18) de Gennes, P.-G. *J. Chem. Phys.* **1980**, *72*, 4756.
(19) Pincus, P. *J. Chem. Phys.* **1981**, *75*, 1996.
(20) Binder, K. *J. Chem. Phys.* **1983**, *79*, 6387.
(21) Binder, K. *Phys. Rev. A* **1984**, *29*, 341.
(22) Strobl, G. R. *Macromolecules* **1985**, *18*, 558.
(23) Schichtel, T. E., Binder, K. *Macromolecules* **1987**, *20*, 1671.
(24) Onuki, A. *J. Chem. Phys.* **1986**, *85*, 1122.
(25) Ohta, T., Nazaki, H., preprint, 1989.
(26) Gunton, J. D.; San Miguel, M.; Sahni, P. S. In *Phase Transitions and Critical Phenomena*; Domb, C., Lebowitz, J. L., Eds.) Academic Press: London, 1983; Vol. 8, p 267.
(27) Doi, M.; Edwards, S. F. *The Theory of Polymer Dynamics*; Clarendon Press: Oxford, 1986.
(28) Cahn, J. W. *Acta Metall.* **1961**, *9*, 795.
(29) Cook, H. E. *Acta Metall.* **1970**, *18*, 297.
(30) Brochard, F.; Jouffroy, J.; Levinson, P. *Macromolecules* **1983**, *16*, 1638.
(31) Kramer, E. J., Green, P. J.; Palmstrom, C. J. *Polymer* **1984**, *25*, 473.
(32) Sillescu, H. *Makromol. Chem., Rapid Commun.* **1984**, *5*, 519.
(33) Brochard, F.; de Gennes, P.-G. *Europhys. Lett.* **1986**, *1*, 221.
(34) Akcasu, A. Z.; Benmouna, M.; Benoit, H. *Polymer* **1986**, *27*, 1935.
(35) Brochard-Wyart, F. *C. R. Acad. Sci. Ser. 2* **1987**, *305*, 657.
(36) Hess, W.; Akcasu, A. Z. *J. Phys. (Paris)* **1988**, *49*, 1261.
(37) Kehr, K. W.; Binder, K.; Reulein, S. M. *Phys. Rev.* **1989**, *B39*, 4891.
(38) Jilge, W.; Carmesin, I.; Kremer, K.; Binder, K. preprint, 1989.
(39) Marro, J.; Bortz, A. B.; Kalos, M. H.; Lebowitz, J. L. *Phys. Rev.* **1975**, *B12*, 2000.
(40) Binder, K.; Kalos, M. H., Lebowitz, J. L.; Marro, J. *Adv. Colloid Interface Sci.* **1979**, *10*, 173.
(41) Lebowitz, J. L.; Marro, J.; Kalos, M. H. *Acta Metall.* **1982**, *30*, 297.
(42) Heermann, D. W. *Phys. Rev. Lett.* **1984**, *52*, 1126.
(43) Amar, J. G.; Sullivan, F. E.; Mountain, R. *Phys. Rev.* **1988**, *B37*, 196.
(44) Kremer, K.; Binder, K. *Comput. Phys. Rep.* **1988**, *7*, 259.
(45) Binder, K. *Colloid Polym. Sci.* **1988**, *266*, 871.
(46) Binder, K. In *Molecular Level Calculations of the Structure and Properties of Non-Crystalline Polymers*; Bicerano, J., Ed.; Marcel Dekker: New York, 1991.
(47) Baumgärtner, A.; Heermann, D. W. *Polymer* **1986**, *27*, 1777.
(48) Sariban, A.; Binder, K. *Polym. Commun.* **1989**, *30*, 205.
(49) Sariban, A.; Binder, K. *Macromolecules* **1988**, *21*, 711.
(50) Sariban, A.; Binder, K. *Colloid Polym. Sci.* **1989**, *267*, 469.
(51) Flory, P. J. *Principles of Polymer Chemistry*; Cornell University Press: Ithaca, NY, 1953.
(52) de Gennes, P.-G. *Scaling Concepts in Polymer Physics*; Cornell University Press: Ithaca, NY, 1979.
(53) For a recent review of Flory–Huggins theory and its extensions, see: Koningsveld, R.; Kleintjens, L. A.; Nies, E. *Croat. Chim. Acta* **1987**, *60*, 53.
(54) Sariban, A.; Binder, K. *Makromol. Chem.* **1988**, *189*, 2357.
(55) Sariban, A.; Binder, K. *J. Chem. Phys.* **1987**, *86*, 5859.
(56) Schwahn, D.; Mortensen, K.; Yee-Madeira, H. *Phys. Rev. Lett.* **1987**, *58*, 1544.
(57) Schwahn, D.; Mortensen, K.; Springer, T.; Yee-Madeira, H.; Thomas, R. *J. Chem. Phys.* **1987**, *87*, 6078.
(58) Khwaja, Y.; Binder, K., preprint, 1989.
(59) Lifshitz, I. M.; Slyozov, V. V. *J. Phys. Chem. Solids* **1961**, *19*, 35.
(60) Siggia, E. *Phys. Rev.* **1979**, *A20*, 595.
(61) Binder, K.; Stauffer, D. *Phys. Rev. Lett.* **1974**, *33*, 1006.
(62) Binder, K.; Kalos, M. H. *J. Stat. Phys.* **1980**, *22*, 363.
(63) Binder, K.; Billotet, C.; Mirold, P. **1978**, *30*, 183.
(64) Binder, K.; Heermann, D. W. *Monte Carlo Simulation in Statistical Physics: An Introduction*; Springer: Berlin-Heidelberg, **1988**.
(65) Binder, K.; Müller-Krumbhaar, H. *Phys. Rev.* **1974**, *B9*, 2328.
(66) Binder, K. *Ann. Phys. (N.Y.)* **1976**, *98*, 390.
(67) Chakrabarti, B. K.; Gunton, J. D. *Phys. Rev. Lett.* **1989**, *63*, 2072.